Twist expansion of the nucleon structure functions, F_2 and F_L, in the DGLAP improved saturation model

Jochen Bartels[(a)], Krzysztof Golec-Biernat[(b,c)] and Leszek Motyka[(a,d)]

[a] *II Institute for Theoretical Physics, Hamburg University, Luruper Chaussee 149, 22761 Hamburg, Germany*

[b] *Institute of Physics, University of Rzeszów, Al. Rejtana 16 A, 35-959 Rzeszów, Poland*

[c] *Institute of Nuclear Physics Polish Academy of Sciences, Radzikowskiego 152, 31-342 Kraków, Poland*

[d] *Institute of Physics, Jagiellonian University, Reymonta 4, 30-059 Kraków, Poland*

(Dated: November 10th, 2009)

Higher twist effects in the deeply inelastic scattering are studied. We start with a short review of the theoretical results on higher twists in QCD. Within the saturation model we perform a twist analysis of the nucleon structure functions F_T and F_L at small value of the Bjorken variable x. The parameters of the model are fitted to the HERA F_2 data, and we derive a prediction for the longitudinal structure function F_L. We conclude that for F_L the higher twist corrections are sizable whereas for $F_2 = F_T + F_L$ there is a nearly complete cancellation of twist-4 corrections in F_T and F_L. We discuss a few consequences for future LHC measurements.

arXiv:0911.1935v1 [hep-ph] 10 Nov 2009

I. INTRODUCTION

A deeper understanding of the transition region at low Q^2 and small x in deep inelastic electron proton scattering has been one of the central tasks of HERA physics. Approaching the transition region from the perturbative side one expects to see the onset of corrections to the successful DGLAP description — in particular those which belong to higher twist operators in QCD. The twist expansion defines a systematic approach and, therefore, provides an attractive framework of investigating the region of validity of the leading twist DGLAP evolution equations.

The essentials of the theory of higher twist operators and their Q^2 evolution have been laid down several years ago, [1, 2, 3]. First, a choice has to be made of a complete operator basis [2, 3], and for their evolution [1] one needs to compute evolution kernels which, for partonic operators in leading order, reduce to $2 \to 2$ scattering kernels. The problem of mixing between different operators has also been addressed first in [1]. In the small-x region at HERA one expects the gluonic operators to be the most dominant ones; so far, a theoretical study of the evolution of twist-4 gluon operators is available only in the double logarithmic approximation [4, 5, 6, 7]. An extensive recent theoretical study of QCD evolution of the higher twist operators can be found in [8].

Numerical studies of the size of potential higher twist corrections [9, 10] indicate that twist-4 corrections to F_2 are small down to $Q^2 \sim 1$ GeV^2, $x \sim 10^{-4}$. A first theoretical analysis [11] applied to HERA data, however, has shown that the situation is more subtle, and from the smallness of twist-4 corrections to F_2 one cannot conclude that contributions of twist-4 operators are small. The simplest QCD diagrams contributing to the twist four gluon operator are shown in Fig. 1: a quark loop couples, via the exchange of four t-channel gluons, to the proton target. Calculating the contribution of these diagrams to the $\gamma^* p$ cross section at small x, and isolating the twist-4 contribution one arrives at the conclusion that the contributions to longitudinal polarized photon has the opposite sign compared to the transversely polarized photon. This implies the possibility that, in $F_2 = F_L + F_T$ which sums over transverse and longitudinal photons, there is a (partial) cancellation of twist four corrections, whereas the twist-4 corrections to F_L or F_T are larger than the corresponding corrections to F_2.

In order to decide whether the HERA data support this possibility, in [11] the saturation model of Golec-Biernat and Wüsthoff [12, 13] which successfully describes the HERA data has been used to obtain a quantitative estimate of twist-4 and even higher twist corrections. This mathematically fairly simple model has four parameters which are fixed by adjusting the model to describe well the HERA F_2 data. The model leads to the total cross sections that exhibit the geometric scaling [14]. The cross sections obtained in the model may be expanded in powers of $\frac{Q_0^2}{Q^2}\left(\frac{1}{x}\right)^{\lambda}$. It was natural to identify the first two terms of this expansion as 'leading twist-2' and 'twist-4 correction',

respectively. Despite its simplicity this model is close enough to the lowest order QCD calculations and supports the sign structure of the twist-4 correction to the transverse and longitudinal cross sections mentioned before. On a quantitative level, the twist-4 corrections to F_L and F_T were found to be sizable, whereas in F_2 they almost cancel. The overall smallness to the $1/Q^2$ corrections to F_2 is consistent with the estimate of [9, 10]: the analysis in [11] therefore provides a natural explanation of the suppression of twist-4 corrections to F_2, without demanding that the higher twist contribution is small for F_L or F_T.

This original version of the GBW model did not include any QCD evolution. Therefore, the connection of this model with evolution of twist four operators in QCD is not possible, and, in particular, the identification of the first and the second term in the $1/Q^2$ expansion as the 'leading' and the 'next-to-leading' twist seems somewhat crude. A more recent version [15] of the GBW model includes QCD evolution and its description of HERA data is slightly better than that of the original model. It is therefore natural to investigate to what extent this improved model exhibits the structure expected for higher twist operators, and then to perform a numerical analysis similar to [11]. This is the goal the present paper.

Our numerical analysis shows an interesting pattern of the higher twist effects in the structure functions. The corrections are sizable in F_L, for the kinematic range relevant for HERA data at low Q^2, 1.8 GeV^2 $<$ 10 GeV^2 and small x, the twist-4 corrections are found to reduce the leading twist result by about 20$-$50%. We compare the obtained predictions for F_L to recent HERA data [16], both for the complete saturation model and its leading twist component. For F_2 the higher twist effects are found to be surprisingly small, at a few percent level down to $Q^2 = 1$ GeV^2.

The paper is organized as follows. The first, longer part in Secs. II–VI is devoted to discussion of theoretical issues, and the second part, in Secs. VII–IX , to the phenomenological applications. In section II we review simple QCD calculations of higher twist corrections in momentum space, restricting ourselves to the double logarithmic approximation, and in section III we reformulate these results in the QCD dipole picture. Next we turn to the saturation model: after a brief review of the simple GBW model in section IV, we perform a theoretical twist analysis of the QCD improved dipole model in section V–VI. The second part (section VII–IX) contains our numerical analysis and discussions of the results and possible consequences for physics at the LHC. Conclusions are given in section X.

II. THE DOUBLE LEADING-LOG APPROXIMATION IN QCD

In this section we give a brief overview of higher twist corrections in small-x QCD. We consider the scattering of a virtual photon with transverse or longitudinal polarization on a quark, and we restrict ourselves to the leading behavior at large Q^2 and small x (double logarithmic approximation, DLA). In this limit, we can either start from the leading-log Q^2 limit and then take the small-x limit or, alternatively, start from the small-x limit and then investigate the large-Q^2 approximation. We begin with the latter one, i.e. we restrict ourselves to those diagrams which have the maximal number of logarithms in $1/x$.

A. Twist 4 corrections

In the small-x limit, the scattering of a virtual photon on a quark is described by the exchange of 2 or more gluons between a closed quark loop and the target quark. For two t-channel gluons, the coupling to the virtual photon is described by the well-known photon impact factor, $D_{(2,0);T,L}(Q;\boldsymbol{k},\boldsymbol{q}-\boldsymbol{k})$, where the subscripts T, L refer to the polarizations of the virtual photon, and $\boldsymbol{k}$ and $\boldsymbol{q}-\boldsymbol{k}$ are the transverse momenta of the two t-channel gluons. In the deep inelastic limit: $q^2 = 0$, $k^2 \ll Q^2$ we have [17, 18]:

$$\begin{aligned} D_{(2,0);T}(Q;\boldsymbol{k},-\boldsymbol{k}) &= A_0\Big(\tfrac{4}{3}\tfrac{k^2}{Q^2}\log\tfrac{Q^2}{k^2} + \tfrac{14}{9}\tfrac{k^2}{Q^2} + \tfrac{2}{5}(\tfrac{k^2}{Q^2})^2 + \mathcal{O}((\tfrac{k^2}{Q^2})^3)\Big) \\ D_{(2,0);L}(Q;\boldsymbol{k},-\boldsymbol{k}) &= A_0\Big(+ \tfrac{2}{3}\tfrac{k^2}{Q^2} - \tfrac{4}{15}(\tfrac{k^2}{Q^2})^2\log\tfrac{Q^2}{k^2} - \tfrac{94}{225}(\tfrac{k^2}{Q^2})^2 + \mathcal{O}((\tfrac{k^2}{Q^2})^3)\Big) \end{aligned} \tag{1}$$

where $A_0 = \sum e_f^2 \alpha_s \frac{\sqrt{8}}{2\pi}$. The leading power, $\left(k^2/Q^2\right)$, belongs to leading twist, the terms proportional to $\left(k^2/Q^2\right)^2$ to twist four etc. These results, obtained directly from Feynman diagrams in the momentum space, lead to estimates of twist contributions to F_T and F_L consistent with estimates of the saturation model, discussed later, in Sec. III and Sec. IV, obtained in the Mellin representation. Important features of $D_{(2,0);T,L}$ are the logarithms and signs of the $\left(k^2/Q^2\right)^2$ corrections: whereas for transverse polarization there is no logarithmic enhancement and the power correction is positive, for longitudinal polarization we have a logarithmic enhancement, and compared to the transverse

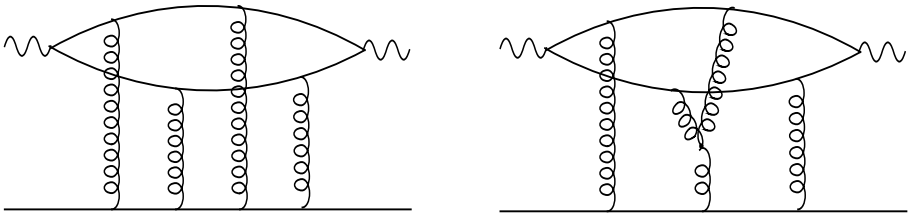

FIG. 1: Two diagrams with four t-channel gluons.

case is has the opposite sign. These simple observations open the possibility that, in F_L, the higher twist corrections are large and that, in the structure function F_2 which sums over transverse and longitudinal polarizations of the photon:

$$F_2 = F_T + F_L, \tag{2}$$

the total twist-four corrections may be small due to cancellations. Within the model to be discussed in this paper we will find that, for the HERA data, this is indeed the case.

The simplest diagram for corrections due to the exchange four gluons (order $\mathcal{O}(g^8)$) is illustrated in Fig. 1, left. In addition to this exchange diagrams, there are diagrams involving the triple gluon vertex, like e.g. the diagram shown in Fig. 1, right.

An efficient method of calculating the sum of all these contributions in the high energy or small-x limit is the effective action, defined in [19] and further studied in [20]. As a result we have, for all diagrams up to order g^8, two classes of contributions:
(a) the BFKL ladders [21, 22, 23, 24], expanded up to order g^8. This includes NLO corrections to the gluon trajectory as well as NLO corrections to the BFKL kernel which, in the leading log approximation, will not be considered; (b) the exchange of four t-channel gluons, where the eikonal couplings to the quark loop at the top and to the quark line at the bottom are fully symmetrized, both in color and in their momentum structure. The coupling to the quark loop, $D^{sym}_{(4,0);T,L}(\boldsymbol{k}_1,\boldsymbol{k}_2,\boldsymbol{k}_3,\boldsymbol{k}_4)$, can be expressed in terms of D_2:

$$\begin{aligned} D_{(4,0);T,L}{}^{a_1a_2a_3a_4}_{sym}(\boldsymbol{k}_1,\boldsymbol{k}_2,\boldsymbol{k}_3,\boldsymbol{k}_4) &= -g^2 d^{a_1a_2a_3a_4}{}_{\rm sym} \\ \times \big(D_{(2,0);T,L}(\boldsymbol{k}_1+\boldsymbol{k}_2+\boldsymbol{k}_3,\boldsymbol{k}_4) &+ D_{(2,0);T,L}(\boldsymbol{k}_2+\boldsymbol{k}_3+\boldsymbol{k}_4,\boldsymbol{k}_1) \\ + D_{(2,0);T,L}(\boldsymbol{k}_3+\boldsymbol{k}_4+\boldsymbol{k}_1,\boldsymbol{k}_2) &+ D_{(2,0);T,L}(\boldsymbol{k}_4+\boldsymbol{k}_1+\boldsymbol{k}_2,\boldsymbol{k}_3) \\ - D_{(2,0);T,L}(\boldsymbol{k}_1+\boldsymbol{k}_2,+\boldsymbol{k}_3+\boldsymbol{k}_4) - D_{(2,0);T,L}(\boldsymbol{k}_1+\boldsymbol{k}_3,\boldsymbol{k}_2+\boldsymbol{k}_4) &- D_{(2,0);T,L}(\boldsymbol{k}_1+\boldsymbol{k}_4,\boldsymbol{k}_2+\boldsymbol{k}_3)\big)\,, \end{aligned} \tag{3}$$

where a_i and $\boldsymbol{k}_i$, $i=1,\ldots,4$ are the color indexes and transverse momenta of the gluons. The color factor has the form:

$$d^{a_1a_2a_3a_4}{}_{\rm sym} = \Big[tr\left(t^{a_1}t^{a_2}t^{a_3}t^{a_4}\right) + tr\left(t^{a_4}t^{a_3}t^{a_2}t^{a_1}\right)\Big]_{\rm sym}, \tag{4}$$

where the subscript 'sym' indicates that the color labels are completely symmetrized.

Next let us consider higher order corrections to (a) which, in the leading logarithmic approximation, sum up to the BFKL ladders. Using a Mellin representation for the impact factors $D_{(2,0);T,L}(Q;k,-k)$ and a double Mellin representation for the BFKL Green's function we write the scattering amplitude in the form:

$$D_{2;T,L}(x;Q^2/Q_0^2) = \int \frac{d\omega}{2\pi i}\int \frac{d\nu}{2\pi i}\left(\frac{1}{x}\right)^{\omega}\left(\frac{Q^2}{Q_0^2}\right)^{\nu} D_{(2,0);T,L}(\nu)\frac{1}{\omega-\bar{\alpha}\chi(\nu,0)} \tag{5}$$

where the integration contours run along the imaginary axis, $\bar{\alpha} = \frac{N_c\alpha_s}{\pi}$, the BFKL characteristic function has the form

$$\chi(\nu,0) = 2\psi(1) - \psi(1+\nu) - \psi(-\nu), \tag{6}$$

and Q_0^2 denotes the momentum scale at the target end of the BFKL ladder. The scattering amplitude D_2 can be expanded in powers of Q^2/Q_0^2: the terms in this expansion are due to the poles of $\chi(\nu)$ at negative integer values:

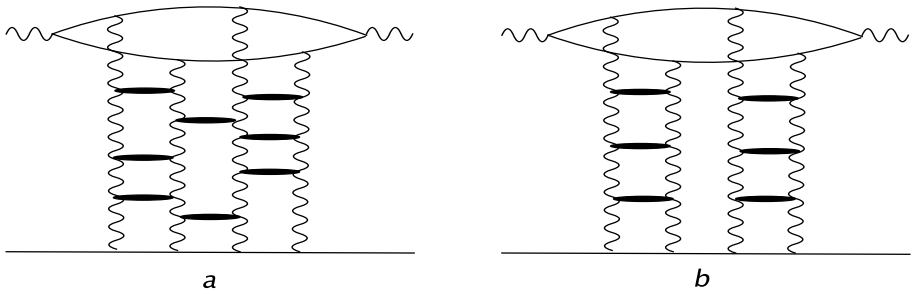

FIG. 2: (a) Pairwise interactions between four reggeized gluons; (b) two noninteracting color singlet ladders.

$\nu = -1, -2, ...$, and the residues of the poles lead to anomalous dimensions. In particular, the pole near $\nu = -1$ leads to the leading twist behavior

$$\left(Q^2/Q_0^2\right)^{\gamma(\omega)}, \ \gamma(\omega) = \frac{N_c \alpha_s}{\pi\omega}, \tag{7}$$

the pole near $\nu = -2$ to the twist four correction

$$\left(Q^2/Q_0^2\right)^{-1+\gamma(\omega)}, \ \gamma(\omega) = \frac{N_c \alpha_s}{\pi\omega}. \tag{8}$$

The exponents are the anomalous dimension of the higher twist operators contained in the BFKL amplitude [25]. In the notation of [1], they belong to the class of non-quasipartonic operators. When coupled to the impact factors $D_{(2,0);T,L}(Q;-k)$, we see from the expansion in (1) that, for the leading-twist terms, the transverse polarization has a logarithmic enhancement compared to the longitudinal polarization. For the twist four correction, the situation is reversed. As to the sign structure, the twist four corrections to transverse and longitudinal polarizations have opposite signs.

Next we turn to higher corrections to class (b). Following the analysis of [1] we consider those corrections which are obtained by inserting all possible pairwise interactions between the reggeized t-channel gluons (Fig. 2a). The large-Q^2 behavior comes from the region where the transverse momenta of the exchanged gluons are ordered and much smaller than the virtuality of the external photon. The leading (in $1/Q^2$) behavior of the four gluon state has been discussed in [5, 6, 7], and we briefly summarize. In the complex ν-plane, the leading singularity is a pole at

$$\gamma_{pole} = \frac{4N_c \alpha_s (1+\delta)}{\pi\omega} \tag{9}$$

where δ is a correction of the order $1/N_c^4$ ($\delta = 0.778/N_c^4$, and for $N_c = 3$, $\delta = 0.0096$). In the large-N_c limit the four gluon state reduces to two noninteracting color singlet gluon ladders, leading to a cut in the ν-plane with the branch point located at

$$\gamma_{cut} = \frac{4N_c \alpha_s}{\pi\omega} \tag{10}$$

The pole in (9) at finite N_c can be viewed as 'bound state' formed by the two color singlet ladders, whereas the cut (10) represents the 'threshold' of two free ladders. The large-Q^2 behavior of this four gluon state is described the evolution equations of the twist four gluon operator in the small-x limit, as discussed in [1]. In the large-N_c limit, the evolution equations reduce to two independent DGLAP ladders.

In order to apply this discussion to the diagrams of class (b) we notice that the twist four contribution of the fermion loop, $D_{(4,0)T,L}$ is easily obtained from (3) and (1). For example, the twist four correction of the transverse polarization is found to be proportional to

$$4g^2 A_0 \frac{2}{5} \frac{\boldsymbol{k}_1 \cdot \boldsymbol{k}_3 \, \boldsymbol{k}_2 \cdot \boldsymbol{k}_4 + \boldsymbol{k}_1 \cdot \boldsymbol{k}_2 \, \boldsymbol{k}_3 \cdot \boldsymbol{k}_4 + \boldsymbol{k}_1 \cdot \boldsymbol{k}_4 \, \boldsymbol{k}_2 \cdot \boldsymbol{k}_3}{(Q^2)^2}, \tag{11}$$

and analogous results are found for the longitudinal polarization. In this way, the four gluon state corrections to transverse and longitudinal polarizations follow the same pattern as the twist four piece inside the BFKL ladder:

compared to transverse polarization, the longitudinal polarization has a logarithmic enhancement and comes with the opposite sign.

Compared to the BFKL-singularity in (8), both in (9) and in (10) the coefficients of the pole at $\omega = 0$ are larger by a factor 4: at small x, this twist-4 correction will therefore dominate. This suggests to consider, within a twist expansion in the small-x region, as a first set of higher twist corrections these four gluon states, disregarding the higher twist contributions of non-quasipartonic operators. It is not difficult to generalize this selection to six, eight etc gluon states. If, in addition, one invokes the large-N_c expansion where the $2n$-gluon state is approximated by n noninteracting color singlet ladders, one arrives at the eikonal picture of multi-Pomeron exchange, which underlies the saturation model to be discussed further below. We shall see that this model embodies many of the features of these n-ladder exchanges, in particular the correct Q^2-evolution.

B. Higher twists in the Balitsky-Kovchegov equation

So far we have discussed a selected subclass of QCD diagrams giving rise to twist-4 corrections to the proton structure functions. It should, however, be kept in mind that this selection of higher twist corrections is not in agreement with what one obtains from summing all leading-$\log 1/x$ contributions from the BFKL Pomeron fan diagrams. This summation may be performed using the Balitsky-Kovchegov (BK) equation [26, 27, 28]. To illustrate this, we summarize the results of the complete small-x analysis which can be found in [4, 29, 30]. The sum of all diagrams contributing to the leading logarithmic $1/x$ approximation can be organized in two classes.
(i) BFKL ladders consisting of reggeized gluons. At the lower end, reggeized gluons can split into two or three elementary gluons. In the former case, the color structure of the splitting is described by a structure constant $f_{ca_1a_2}$, in the latter case by the product of two structure constants, e.g. $f_{ca_1d}f_{da_2a_3}$.
(ii) BFKL-like ladders where, instead of the reggeized gluons which belong to the adjoint color representation, we have Reggeons in the symmetric octet and singlet color representations. In both cases, the trajectory functions are the same as for the reggeized gluon. The corresponding color tensors are listed in [29]. The sum of these diagrams is symmetric under the exchange of momenta and color indexes.
(iii) Diagrams with a four gluon t-channel state. This state is symmetric under the exchange of t-channel gluons (momenta and color indexes). There is no direct coupling of this state to the quark loop at the top. Instead, through the $2 \to 4$ reggeized gluon vertex it couples to a BFKL ladder which then connects with the quark loop (Fig. 3). Class (i) and (ii) represent the all-order generalizations of (a) and (b), respectively, whereas (iii) starts at the order g^{10}. In [29], (i) and (ii) are denoted by D_4^R, class (iii) by D_4^I.

As we have already stated, in (iii) the four gluon state that we have discussed before does not couple directly to the quark loop: the coupling goes through a BFKL ladder and a $2 \to 4$ transition vertex. Making use of the large-Q^2 results discussed before, we interpret this as a mixing between the non-quasipartonic twist four piece inside the BFKL ladder and the twist four gluon operator. A detailed analysis [30], however, shows that, at the leading logarithmic $\log Q^2$, approximation, this transition kernel between the two twist-4 operators, in the large-N_c limit, vanishes. This also holds for the transition of the twist-6 piece inside the BFKL ladder to the twist-6 piece in the four gluon state. Generalizing this to more than four t-channel gluons, one arrives at the conclusion that, in the double leading logarithmic approximation, the contribution of higher twists given by the BK fan diagrams vanishes, and only propagation of two interacting t-channel gluons contributes to the amplitudes. Note however that this result is only valid in the large-N_c limit.

Therefore, from a theoretical point of view, the twist expansion derived from the selection of diagrams with $2n$ t-channel gluons in the large-N_c limit should be viewed as being different from descriptions based upon the BK equation.

III. COLOR DIPOLE PICTURE

It is important to emphasize that, in the small-x limit, for the class of QCD diagrams which we have discussed, the scattering amplitude for the elastic scattering of a virtual photon on a quark can be cast into the dipole form [31]:

$$\sigma_{T,L}^{\gamma^* p}(x,Q^2) \;=\; \sum_f \int d^2\mathbf{r} \int_0^1 dz \; |\Psi_{T,L}^f(z,r,Q^2)|^2 \; \sigma(x,\mathbf{r}) \tag{12}$$

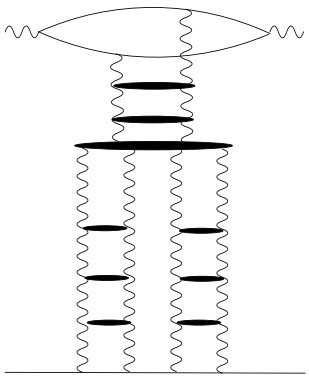

FIG. 3: A fan diagram.

where T and L denote the virtual photon polarization: transverse and longitudinal, respectively. The light-cone photon wave function, $\Psi^f_{T,L}$, is modeled by the lowest order $\gamma^* g \to q\bar{q}$ scattering amplitudes which give

$$|\Psi^f_T(z,r,Q^2)|^2 \;=\; \frac{2N_c\alpha_{em}e_f^2}{4\pi^2}\left\{\left[z^2+(1-z)^2\right]\epsilon^2\,K_1^2(\epsilon r)+m_f^2\,K_0^2(\epsilon r)\right\} \tag{13}$$

$$|\Psi^f_L(z,r,Q^2)|^2 \;=\; \frac{8N_c\alpha_{em}e_f^2}{4\pi^2}\,Q^2z^2(1-z)^2\,K_0^2(\epsilon r) \tag{14}$$

where $K_{0,1}$ are the Bessel–McDonald functions, $\epsilon^2 = z(1-z)Q^2+m_f^2$ and $r=|\mathbf{r}|$. The measured structure functions are related to $\sigma^{\gamma^* p}_{T,L}(x,Q^2)$ by the standard formula

$$F_{T,L} = \frac{Q^2}{4\pi^2\alpha_{em}} \tag{15}$$

In (12), all details describing the interaction of the quark-antiquark pair with the target quark are contained in the dipole cross section, $\sigma(x,\mathbf{r})$. In particular, the exchange of two non-interacting color singlet gluon ladders provides a contribution proportional to the product of two gluon structure functions, $(xg(x,C/r^2))^2$.

Important characteristics of the twist expansion follow from the structure of the photon wave functions and do not depend upon the details of $\sigma(x,\mathbf{r})$. This is most easily seen by taking the Mellin transform of (12). In general, the Mellin transform of a function $f(r^2)$ is defined as

$$\tilde{f}(s) \equiv \mathcal{M}_{r^2}\left[f(r^2)\right](s) \;=\; \int_0^\infty dr^2\,(r^2)^{s-1}\,f(r^2) \tag{16}$$

while the inverse relation reads

$$f(r^2) \;=\; \int_C \frac{ds}{2\pi i}\,(r^2)^{-s}\,\tilde{f}(s) \tag{17}$$

where the integration contour C lays in the fundamental strip of the Mellin transform to be discussed below.

Let us write Eq. (12) in the following form

$$\sigma^{\gamma^* p}_{T,L}(x,Q^2) \;=\; \int_0^\infty \frac{dr^2}{r^2}\,H_{T,L}(r,Q^2)\,\sigma(x,r) \tag{18}$$

where

$$H_{T,L}(r,Q^2) \;\equiv\; \pi r^2\sum_f\int_0^1 dz\,|\Psi^f_{T,L}(z,r,Q^2)|^2\,. \tag{19}$$

Substituting the inverse Mellin transform of the dipole cross section,

$$\sigma(x,r) \;=\; \int_C \frac{ds}{2\pi i}\,(r^2Q_0^2)^{-s}\;\tilde{\sigma}(x,s) \tag{20}$$

we find the Mellin representation of the $\gamma^* p$ cross sections, given by the Parseval formula

$$\sigma_{T,L}^{\gamma^* p}(x,Q^2) \;=\; \int\limits_{C_s} \frac{ds}{2\pi i}\, \tilde{\sigma}(x,s)\, \tilde{H}_{T,L}(-s, Q^2/Q_0^2) \tag{21}$$

where $\tilde{H}_{T,L}(-s,Q^2)$ is the Mellin transform of $H_{T,L}(r,Q^2)$. The integration contour C_s in the complex s-plane is placed in the fundamental strip in which the integrals defining $\tilde{\sigma}(x,s)$ and $\tilde{H}_{T,L}(-s,Q^2)$ are convergent. The strip is determined from the following leading behaviour of both functions at small and large values of r (up to logarithms of r):

$$H_{T,L}(r,Q^2) = \begin{cases} \text{const} & \text{for } \; r \to 0, \\ 1/r^{2n} & \text{for } \; r \to \infty \end{cases} \tag{22}$$

with $n = 1$ for transverse and $n = 2$ for longitudinal polarization. For the dipole cross section we take, as an example,

$$\sigma(x,r) \;=\; \begin{cases} r^2 & \text{for } \; r \to 0, \\ \text{const} & \text{for } \; r \to \infty \end{cases} \tag{23}$$

In this case the fundamental strip of $\tilde{\sigma}(x,s)$ is defined by the condition $-1 < \mathrm{Re}\, s < 0$ while the fundamental strip of $\tilde{H}_{T,L}(s,Q^2)$ is given by $0 < \mathrm{Re}\, s < n$. Taking into account the minus sign in $\tilde{H}_{T,L}(-s,Q^2)$, we find that the integration contour C_s in Eq. (21) lays in the strip:

$$-1 < \mathrm{Re}\, s < 0\,. \tag{24}$$

It can be chosen parallel to the imaginary axis, for example, $s = -1/2 + i\nu$ with real ν.

For the Mellin transform of $H_{T,L}(r,Q^2)$ we restrict ourselves to massless quarks, $m_f = 0$. In this case, $H_{T,L}$ are functions of only one combined variable, $\hat{r} = r\,Q$:

$$H_T(\hat{r}) \;=\; A_0 \int_0^1 dz\, [z^2 + (1-z)^2]\, z(1-z)\, \hat{r}^2 K_1^2(\sqrt{z(1-z)}\,\hat{r}) \tag{25}$$

$$H_L(\hat{r}) \;=\; 4A_0 \int_0^1 dz\, z^2(1-z)^2\, \hat{r}^2 K_0^2(\sqrt{z(1-z)}\,\hat{r})\,. \tag{26}$$

where we introduced $A_0 = N_c \alpha_{em} \langle e^2 \rangle / (2\pi)$ and $\langle e^2 \rangle = \sum_f e_f^2$. In Appendix A we found the Mellin transforms of these functions in the form

$$\tilde{H}_{T,L}(s,Q^2) \;=\; \left(\frac{Q^2}{4}\right)^{-s} \tilde{H}_{T,L}(s) \tag{27}$$

with $\tilde{H}_{T,L}(s)$ given by Eqs. (A9) and (A10):

$$\tilde{H}_T(s) \;=\; \frac{A_0\,\pi}{8}\, \frac{\Gamma(2+s)\,\Gamma(1+s)\,\Gamma(s)\,\Gamma(1-s)\,\Gamma(3-s)}{\Gamma(3/2+s)\,\Gamma(2-s)\,\Gamma(5/2-s)}\,. \tag{28}$$

and

$$\tilde{H}_L(s) \;=\; \frac{A_0\,\pi}{4}\, \frac{(\Gamma(1+s))^3\,\Gamma(2-s)}{\Gamma(3/2+s)\,\Gamma(5/2-s)}. \tag{29}$$

Both functions have simple or multiple poles for negative and positive real values of s.

Substituting these results into Eq. (21) we obtain

$$\sigma_{L,T}^{\gamma^* p}(x,Q^2) \;=\; \int\limits_{C_s} \frac{ds}{2\pi i} \left(\frac{Q_0^2}{Q^2}\right)^{-s} \tilde{\sigma}(x,s)\; \tilde{H}_{T,L}(-s) \tag{30}$$

with the contour C_s in the fundamental strip (24). The twist expansion is obtained by closing the s-contour to the left. The functions $\tilde{H}_{T,L}(s)$ have single poles to the right of C at positive integers, except for the regular points

at $s = 2$ for transverse and $s = 1$ for longitudinal polarizations. Thus, both functions have the following Laurent expansion around each singular point $s = n$:

$$\tilde{H}_{T,L}(s) \;=\; \frac{a_{T,L}^{(n)}}{s-n} \;+\; b_{T,L}^{(n)} \;+\; \mathcal{O}\,(s-n) \tag{31}$$

with

$$\begin{aligned} a_T^{(1)} \;&=\; -\frac{2}{3}A_0, \\ a_T^{(2)} \;&=\; 0,\; b_T^{(2)} = -\frac{4}{5}A_0 \end{aligned} \tag{32}$$

and

$$\begin{aligned} a_L^{(1)} \;&=\; 0,\; b_L^{(1)} = \frac{2}{3}A_0 \\ a_L^{(2)} \;&=\; -\frac{16}{15}A_0. \end{aligned} \tag{33}$$

Assuming, for simplicity, that to the left of C_s, $\tilde{\sigma}(x,s)$ has only poles at $s = -1, 2, ...$ (the more realistic case where $\tilde{\sigma}$ has cuts in the complex s-plane will be discussed further below), we close the contour to the left and arrive at the twist expansion:

$$\sigma_{L,T}^{\gamma^* p}(x,Q^2) \;=\; \sum_{n=1}^{\infty} \sigma_{T,L}^{(\tau=2n)}(x,Q^2)\,. \tag{34}$$

where $\sigma^{(\tau=2n)} \sim 1/Q^{2n}$ (modulo powers of $\log Q^2$). With (28) and (29) we obtain:

$$\sigma_{T,L}^{(\tau=2n)} \;=\; \int\limits_{C_n} \frac{ds}{2\pi i} \left(\frac{Q_0^2}{Q^2}\right)^{-s} \tilde{\sigma}(x,s) \left\{ \frac{-a_{T,L}^{(n)}}{s+n} \;+\; b_{T,L}^{(n)} + \ldots \right\} \tag{35}$$

where the dots stand for terms regular at $s = -n$. In particular, for the twist-4 corrections we re-discover the previous result from (1):
(i) due to the vanishing of $a_T^{(2)}$, the longitudinal structure function is enhanced,
(ii) the leading terms in F_T and F_L come with opposite signs.

For completeness, we also consider the complex half s-plane to the right of the contour C. It is well known that the Bessel-McDonald functions $K_\nu(x)$ have a convergent expansion around $x = 0$, whereas for large arguments the expansion in powers of $1/x$ is asymptotic. Therefore, writing the functions $H_{T,L}(\hat{r})$ in the form

$$H_T(\hat{r}) \;=\; \frac{A_0\pi}{8} \int\limits_C \frac{ds}{2\pi i} \left(\frac{\hat{r}^2}{4}\right)^{-s} \frac{\Gamma(2+s)\,\Gamma(1+s)\,\Gamma(s)\,\Gamma(1-s)\,\Gamma(3-s)}{\Gamma(3/2+s)\,\Gamma(2-s)\,\Gamma(5/2-s)} \tag{36}$$

$$H_L(\hat{r}) \;=\; \frac{A_0\pi}{4} \int\limits_C \frac{ds}{2\pi i} \left(\frac{\hat{r}^2}{4}\right)^{-s} \frac{(\Gamma(1+s))^3\,\Gamma(2-s)}{\Gamma(3/2+s)\,\Gamma(5/2-s)}\,, \tag{37}$$

we conclude that the expansion in powers of $\hat{r}$ — which is obtained by closing the contour to the left — is convergent. In contrast, the expansion in powers of $1/\hat{r}$ — which corresponds to closing the contour to the right and computing residues of the poles at positive integers — leads to a divergent result which form an asymptotic series for $H_{T,L}(\hat{r})$ when $\hat{r}^2 \to \infty$:

$$H_{T,L}(\hat{r}) \;\sim\; \frac{h_{T,L}^{(1)}}{\hat{r}^2} + \frac{h_{T,L}^{(2)}}{\hat{r}^4} + \frac{h_{T,L}^{(3)}}{\hat{r}^6} \;+\ldots, \tag{38}$$

where the coefficients $h_{T,L}^{(n)} \sim a_{T,L}^{(n)}$ are equal to:

$$h_T^{(1)} \;=\; \tfrac{8}{3}A_0\,, \qquad h_T^{(2)} = 0\,, \qquad h_T^{(3)} = \tfrac{3072}{35}A_0 \tag{39}$$

$$h_L^{(1)} \;=\; 0\,, \qquad h_L^{(2)} = \tfrac{256}{15}A_0\,, \qquad h_L^{(3)} = \tfrac{9216}{35}A_0\,. \tag{40}$$

This asymptotic expansion justifies the large-r behaviour of $H_{T,L}(r,Q^2)$ used in the determination of the fundamental strip (24). Moreover, returning to (21) we conclude that, because of the negative sign of the argument of $\tilde{H}_{T,L}$, the twist expansion is an asymptotic expansion.

In conclusion, the opposite sign structure as well as the relative enhancement of the twist-4 corrections to F_L are general features of the small-x limit in QCD, and they provide the possibility that the total twist-4 correction to F_2 may become small. In the following we choose, for a quantitative estimate, a particular model, the QCD improved dipole model.

IV. THE MODEL

We aim for the construction of the twist expansion of the proton structure functions F_T and F_L at small values of the Bjorken variable x. The starting point for our following analysis is the GBW saturation model [12] and its QCD improved version which incorporates the leading logarithmic DGLAP evolution [15].

The standard formula defining the total cross section for the scattering of a virtual photon $\gamma^*_{T,L}(Q^2)$ on a proton p at small value of the Bjorken variable x has already been written down in (12). The function $\sigma(x,\mathbf{r})$ in Eq. (12) is the color dipole cross section, describing the interaction of the $q\overline{q}$ pair with the proton. In the original GBW formulation [12] it depends on the dipole size r and the Bjorken variable x, and takes the following form

$$\sigma(x,r) \;=\; \sigma_0 \left\{1 - \exp\left(-r^2 Q^2_{\rm sat}(x)/4\right)\right\} \tag{41}$$

where $Q^2_{\rm sat}$ is a saturation scale which depends on x. After incorporating the DGLAP evolution for small dipole sizes the dipole cross section is modeled in [15] as

$$\sigma(x,r) \;=\; \sigma_0 \left\{1 - \exp\left(-\Omega(x,r^2)\right)\right\} \tag{42}$$

where the opacity

$$\Omega(x,r^2) \;=\; \frac{\pi^2 r^2\, \alpha_s(\mu^2)\, g(x,\mu^2)}{3\sigma_0}\,, \tag{43}$$

and $g(x,\mu^2) \equiv xG(x,\mu^2)$ is the gluon distribution (multiplied by x) which obeys the DGLAP evolution equation (B1) from Appendix B. The evolution scale μ^2 was originally assumed to depend on the dipole size in the following way:

$$\mu^2 \;=\; C/r^2 + \mu_0^2\,. \tag{44}$$

Both models of the dipole cross section are eikonal and follow the Glauber-Mueller formulae. For the remainder of this section, we restrict ourselves to the original GBW model.

Following our discussion of the previous section, we need the Mellin transform of the dipole cross section. In the case of the GBW parameterization (41), we find

$$\begin{aligned}\tilde{\sigma}(x,s) \;&=\; \sigma_0 \int_0^\infty dr^2\, (r^2)^{s-1} \left\{1 - \exp\left(-r^2 Q^2_{\rm sat}(x)/4\right)\right\} \\ &=\; -\sigma_0 \left(\frac{Q^2_{\rm sat}}{4}\right)^{-s} \Gamma(s)\,. \end{aligned} \tag{45}$$

Substituting this result, together with relation (27), into Eq. (21), we obtain

$$\sigma^{\gamma^* p}_{L,T}(x,Q^2) \;=\; \sigma_0 \int\limits_{C_s} \frac{ds}{2\pi i} \left(\frac{Q^2_{\rm sat}}{Q^2}\right)^{-s} \{-\Gamma(s)\}\, \tilde{H}_{T,L}(-s) \tag{46}$$

with the contour C_s in the fundamental strip (24). We see that the poles to the left of C_s at negative integers lead to the twist expansion:

$$\sigma^{\gamma^* p}_{L,T}(x,Q^2) \;=\; \sum_{n=1}^{\infty} \sigma^{(\tau=2n)}_{T,L}(x,Q^2)\,. \tag{47}$$

where $\sigma^{(\tau=2n)} \sim 1/Q^{2n}$. Singularities come from the single poles of the Euler gamma function $\Gamma(s)$ and from the poles in $\tilde{H}_{T,L}(-s)$. In particular, encircling the pole at $s=-n$ by a small counter-clockwise oriented contour C_n, and expanding both functions around this point, we obtain

$$\sigma_{T,L}^{(\tau=2n)} = \sigma_0 \int\limits_{C_n} \frac{ds}{2\pi i} \left(\frac{Q_{\rm sat}^2}{Q^2}\right)^{-s} \left\{\frac{\gamma_1^{(n)}}{s+n} + \gamma_0^{(n)} + \ldots\right\} \left\{\frac{-a_{T,L}^{(n)}}{s+n} + b_{T,L}^{(n)} + \ldots\right\} \tag{48}$$

where the dots denote terms regular at $s=-n$. The result of the integration is indeed proportional to $1/Q^{2n}$ with the logarithmic enhancement coming from the double poles

$$\sigma_{T,L}^{(\tau=2n)} = \sigma_0 \frac{Q_{\rm sat}^{2n}}{Q^{2n}} \left\{-\gamma_1^{(n)} a_{T,L}^{(n)} \log(Q^2/Q_{\rm sat}^2) + \left(\gamma_1^{(n)} b_{T,L}^{(n)} - \gamma_0^{(n)} a_{T,L}^{(n)}\right)\right\}. \tag{49}$$

In particular, we find [11] – for twist-2:

$$\sigma_T^{(\tau=2)} = \frac{\alpha_{em}\sigma_0}{\pi} \langle e^2\rangle \frac{Q_{\rm sat}^2}{Q^2} \left\{\log(Q^2/Q_{\rm sat}^2) + \gamma_E + 1/6\right\} \tag{50}$$

$$\sigma_L^{(\tau=2)} = \frac{\alpha_{em}\sigma_0}{\pi} \langle e^2\rangle \frac{Q_{\rm sat}^2}{Q^2} \tag{51}$$

and for twist-4:

$$\sigma_T^{(\tau=4)} = \frac{3}{5}\frac{\alpha_{em}\sigma_0}{\pi} \langle e^2\rangle \frac{Q_{\rm sat}^4}{Q^4} \tag{52}$$

$$\sigma_L^{(\tau=4)} = -\frac{4}{5}\frac{\alpha_{em}\sigma_0}{\pi} \langle e^2\rangle \frac{Q_{\rm sat}^4}{Q^4} \left\{\log(Q^2/Q_{\rm sat}^2) + \gamma_E + 1/15\right\}. \tag{53}$$

Notice the negative sign of $\sigma_L^{(\tau=4)}$ and the lack of logarithm in $\sigma_L^{(\tau=2)}$ and $\sigma_T^{(\tau=4)}$ due to the singularity structure (31) with $a_L^{(1)}=0$ and $a_T^{(2)}=0$.

V. SINGULARITY STRUCTURE OF THE DGLAP IMPROVED MODEL

In the DGLAP improved saturation model, the r-dependence of the dipole cross section, given by Eq. (42), is rather involved and its exact Mellin transform is not known. However, it is still possible to extract the information about the Mellin transform necessary to carry out the twist analysis. For this purpose it is convenient to use a slightly modified definition of the scale μ^2 in Eq. (42):

$$\mu^2 = \begin{cases} C/r^2 & \text{for} \quad r^2 < C/\mu_0^2, \\ \mu_0^2 & \text{for} \quad r^2 \geq C/\mu_0^2. \end{cases} \tag{54}$$

Such a modification preserves all the desired features of the original model and allows to separate the r^2-integration range of the Mellin transform of the dipole cross section $\tilde{\sigma}(x,s)$ into two regions: the *perturbative* one, defined by the condition $r^2 < C/\mu_0^2$, in which the gluon density and strong coupling constant are given by one-loop expressions with the scale $\mu^2 = C/r^2$, and the *soft* region, defined by the condition $r^2 \geq C/\mu_0^2$, where the scale is frozen at $\mu^2=\mu_0^2$: Thus

$$\tilde{\sigma}(x,s) = \tilde{\sigma}_{\rm pert}(x,s) + \tilde{\sigma}_{\rm soft}(x,s). \tag{55}$$

In the soft region the dipole cross section takes the form of the GBW saturation model (41) with the saturation scale

$$Q_{\rm sat}^2(x) = \frac{4\pi^2 \alpha_s(\mu_0^2)\, g(x,\mu_0^2)}{3\sigma_0}. \tag{56}$$

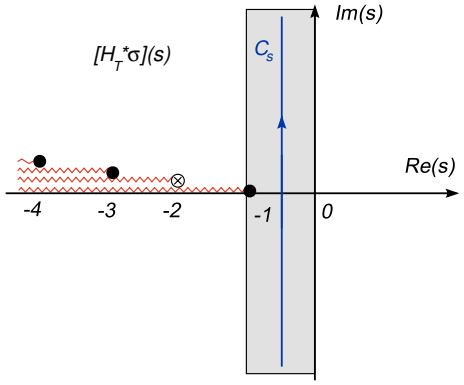

FIG. 4: The singularity structure of $\tilde{\sigma}(x,s)\tilde{H}_T(-s)$ in the complex s-plane to the left of the Mellin integration contour $\mathcal{C}_s$ in the fundamental strip shown as the gray band. The zigzag lines indicate the cuts coming from powers of the Mellin transform of $\alpha_s(\mu^2)g(x,\mu^2)$ while the full circles are the poles of $\tilde{H}_T(-s)$ that coincide with branch points of $\tilde{\sigma}(x,s)$. The crossed circle at $s=-2$ is the branch point that is not accompanied by the pole of $\tilde{H}_T(-s)$.

The contribution from this region to the Mellin transform is given by

$$\begin{aligned}\tilde{\sigma}_{\rm soft}(x,s) &= \int_{C/\mu_0^2}^{\infty} dr^2\,(r^2)^{s-1}\left\{1-\exp\left(-r^2Q_{\rm sat}^2(x)/4\right)\right\}\\ &= -\sigma_0\left(\frac{Q_{\rm sat}^2}{4}\right)^{-s}\left\{\frac{a^s}{s}+\Gamma(s,a)\right\}\end{aligned} \tag{57}$$

where $a=CQ_{\rm sat}^2/(4\mu_0^2)$ and $\Gamma(s,a)$ is the incomplete gamma function which has no singularities in the complex s-plane. The soft part has only a single pole at $s=0$ which does not contribute to the twist expansion.

The contribution from the perturbative region may be computed term by term from the expansion

$$\begin{aligned}\sigma_{\rm pert}(x,r) &= \sum_{n=1}^{\infty}\sigma_{\rm pert}^{(n)}(x,r)\\ &= \sum_{n=1}^{\infty}\sigma_0\,\frac{(-1)^{n+1}}{n!}\,\Omega_{\rm pert}^n(x,r^2)\end{aligned} \tag{58}$$

and the perturbative part of the opacity reads

$$\Omega_{\rm pert}(x,r^2)=\frac{\pi^2}{3\sigma_0}\,r^2\alpha_s(C/r^2)\,g(x,C/r^2)\,\Theta\left(C/r^2-\mu_0^2\right). \tag{59}$$

The Mellin transform $\tilde{\sigma}_{\rm pert}(x,s)$ exists due to the theta distribution and is given by the sum of the Mellin transforms of the subsequent terms in the expansion (58)

$$\tilde{\sigma}_{\rm pert}^{(n)}(x,s)=\sigma_0\,\frac{(-1)^{n+1}}{n!}\,\widetilde{\Omega}_{\rm pert}^n(x,s) \tag{60}$$

Each term contributes a cut singularity in the s-plane extending to the left from the branch point at negative integers, see Fig. 4. The positions of the branch points are determined by the corresponding power of r^2 since the powers of $\alpha_s(\mu^2)g(x,\mu^2)$ do not introduce any additional shift.

For example, we compute first the Mellin transform

$$\mathcal{M}_{r^2}\left[\alpha_s(C/r^2)g(x,C/r^2)\Theta\left(C/r^2-\mu_0^2\right)\right](s)=\left(\frac{C}{\Lambda^2}\right)^s\widetilde{\alpha_s g}(x,s) \tag{61}$$

where $\widetilde{\alpha_s g}$ denotes the Mellin transform with respect to the scale μ^2, defined as

$$\widetilde{\alpha_s g}(x,s)=\int_{\mu_0^2}^{\infty}\frac{d\mu^2}{\mu^2}\left(\frac{\mu^2}{\Lambda^2}\right)^{-s}\alpha_s(\mu^2)g(x,\mu^2). \tag{62}$$

In such a case the inverse relation reads

$$\alpha_s(\mu^2) g(x,\mu^2) \;=\; \int_C \frac{ds}{2\pi i} \left(\frac{\mu^2}{\Lambda^2}\right)^s \widetilde{\alpha_s g}(x,s)\,. \tag{63}$$

where the integration contour lays to the right of the right-most singularity. Using the property of the Mellin transform: $\mathcal{M}_t[t^n f(t)](s) = \mathcal{M}_t[f(t)](s+n)$, we find

$$\mathcal{M}_{r^2}[\Omega_{\rm pert}(x,r^2)](s) \;=\; \frac{\pi^2}{3\sigma_0}\,\left(\frac{C}{\Lambda^2}\right)^{s+1}\,\widetilde{\alpha_s g}(x,s+1) \tag{64}$$

and after substituting solution (B16), we obtain

$$\tilde\Omega_{\rm pert}(x,s) \;=\; \frac{\pi^2}{3\sigma_0}\,\left(\frac{C}{\Lambda^2}\right)^{s+1} \int \frac{d\omega}{2\pi i}\, x^{-\omega}\, \frac{2\pi\,\tilde g_0(\omega)}{\tilde P_{gg}(\omega)}\,(s+1)^{-\frac{b_0}{2\pi}\tilde P_{gg}(\omega)}\,. \tag{65}$$

The logarithmic cut singularity along the negative real axis with the branch point at $s=-1$ is obvious from this solution. The Mellin transform of $\Omega^2_{\rm pert}(x,r^2)$ is given by

$$\mathcal{M}_{r^2}[\Omega^2_{\rm pert}(x,r^2)](s) \;=\; \left(\frac{\pi^2}{3\sigma_0}\right)^2\,\left(\frac{C}{\Lambda^2}\right)^{s+2}\,\widetilde{(\alpha_s g)^2}(x,s+2) \tag{66}$$

$$\;=\; \left(\frac{\pi^2}{3\sigma_0}\right)^2\,\left(\frac{C}{\Lambda^2}\right)^{s+2}\int \frac{ds'}{2\pi i}\,\widetilde{\alpha_s g}(x,s')\,\widetilde{\alpha_s g}(x,s+2-s')\,. \tag{67}$$

where $\widetilde{(\alpha_s g)^2}$ is the Mellin transform (62) of the product $[\alpha_s(\mu^2) g(x,\mu^2)]^2$, and the Mellin convolution theorem was used in the last equality. It can be shown explicitly that expression (66) has a cut singularity along the real axis for $-\infty < s < -2$ with the branch point at $s=-2$.

In general, we have

$$\mathcal{M}_{r^2}[\Omega^n_{\rm pert}(x,r^2)](s) \;=\; \left(\frac{\pi^2}{3\sigma_0}\right)^n\,\left(\frac{C}{\Lambda^2}\right)^{s+n}\,\widetilde{(\alpha_s g)^n}(x,s+n) \tag{68}$$

with the logarithmic cut along the negative real axis starting at the branch point at $s=-n$, see Fig. 4. In summary, the singularity structure of the Mellin transform (55), relevant for the twist expansion, is determined by the perturbative part only.

VI. TWIST DECOMPOSITION IN THE DGLAP IMPROVED MODEL

At each twist the saturation model incorporates a few distinct contributions that have a clear interpretation within perturbative QCD. The contributions may be classified using the singularity structure of the product $\tilde\sigma(x,s)\tilde H_{T,L}(-s,Q^2)$ in the Mellin plane.

A. Twist-2 contributions

Starting from the twist-2 analysis, we close the contour $\mathcal{C}_s$ of the Mellin integration in Eq. (21) with two large quarter-circles $\mathcal{Q}_1$ and $\mathcal{Q}_2$ and a contour $\mathcal{D}_s$ enveloping the complex cut of $\tilde\sigma(x,s)$ with the branch point at $s=-1$, see Fig. 5. Then, we decompose $\tilde\sigma(x,s)$ into a part which singular at $s=-1$, given by $\tilde\sigma^{(1)}_{\rm pert}(x,s) = \sigma_0\tilde\Omega_{\rm pert}(x,s)$, and a part which is regular at this point, $\tilde\sigma^{(s=-1)}_{\rm reg}(x,s)$. The latter part consists both the soft contribution (57) and the contributions from multiple exchanges with cuts starting from $s=-2$. Thus, using expansion (31) for $\tilde H_{T,L}(-s)$ with $n=1$, we obtain the twist-2 part in the form

$$\sigma^{(\tau=2)}_{T,L} \;=\; \int\limits_{-D_s} \frac{ds}{2\pi i}\left(\frac{Q^2}{4}\right)^s \Big\{\sigma_0\,\tilde\Omega_{\rm pert}(x,s) \;+\; \tilde\sigma^{(s=-1)}_{\rm reg}(x,s)\Big\}\,\Big\{\frac{-a^{(1)}_{T,L}}{s+1} \;+\; b^{(1)}_{T,L} \;+\; \mathcal{O}(s+1)\Big\} \tag{69}$$

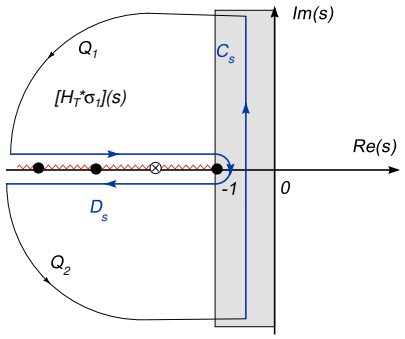

FIG. 5: The discontinuity structure of $\tilde{\sigma}^{(1)}_{\rm pert}(x,s)\tilde{H}_T(-s)$ and the integration contours in the complex s-plane with the pieces: $\mathcal{Q}_1$, $\mathcal{Q}_2$ and D_s. The meaning of all symbols is as in Fig. 4

where the integration contour is reversed with respect to the contour D_s shown in Fig. 5, and the Laurent expansion coefficients

$$a_T^{(1)} = -\tfrac{2}{3}A_0\,, \qquad a_L^{(1)} = 0\,, \qquad b_T^{(1)} = \left(\tfrac{4}{3}\gamma_E - \tfrac{5}{9}\right)A_0\,, \qquad b_L^{(1)} = \tfrac{2}{3}A_0\,. \tag{70}$$

with $A_0 = N_c\alpha_{em}\langle e^2\rangle/(2\pi)$.

Let us compute the twist-2 contribution for transverse photons coming from the most singular part of the Mellin integrand:

$$\Delta_a\sigma_T^{(\tau=2)} \;=\; \sigma_0 \int\limits_{-D_s} \frac{ds}{2\pi i}\left(\frac{Q^2}{4}\right)^s \tilde{\Omega}_{\rm pert}(x,s)\left\{\frac{-a_T^{(1)}}{s+1}\right\}. \tag{71}$$

The analogous longitudinal contribution vanishes since $a_L^{(1)} = 0$. Using relation (64), we find

$$\Delta_a\sigma_T^{(\tau=2)} \;=\; -\frac{4\pi^2 a_T^{(1)}}{3\,Q^2}\int\limits_{-D_s}\frac{ds}{2\pi i}\left(\frac{CQ^2}{4\Lambda^2}\right)^{s+1}\frac{\widetilde{\alpha_s g}(x,s+1)}{s+1}. \tag{72}$$

The contour integration can be computed directly after substituting Eq. (65) or, alternatively, one can realize that the integral in (72) is the inverse Mellin transform (63) at the scale $\mu^2 = CQ^2/4$ of the following function

$$S_T^{(2)}(x,\mu^2) \;=\; \int_{\mu_0^2}^{\mu^2}\frac{d\mu'^2}{\mu'^2}\,\alpha_s(\mu'^2)g(x,\mu'^2) \;+\; S_T^{(2)}(x,\mu_0^2)\,, \tag{73}$$

where the reminder $S_T^{(2)}(x,\mu_0^2)$ depends only on the gluon distribution at an initial scale μ_0^2. It can be computed using the DGLAP equation (B13)

$$S_T^{(2)}(x,\mu_0^2) = \int\limits_{C_\omega}\frac{d\omega}{2\pi i}\,x^{-\omega}\,\frac{2\pi\,\tilde{g}(\omega,\mu_0^2)}{\tilde{P}_{gg}(\omega)}\,. \tag{74}$$

Thus, we finally obtain

$$\Delta_a\sigma_T^{(\tau=2)} \;=\; -\frac{4\pi^2 a_T^{(1)}}{3\,Q^2}\left\{\int_{\mu_0^2}^{CQ^2/4}\frac{d\mu'^2}{\mu'^2}\,\alpha_s(\mu'^2)\,g(x,\mu'^2) \;+\; S_T^{(2)}(x,\mu_0^2)\right\}. \tag{75}$$

The leading logarithmic term in Eq. (75) coincides with the standard DGLAP expression for $\sigma_T^{\gamma^* p}$ obtained assuming that the see quarks come from the gluon splitting in the last step of the evolution.

The higher orders in the Laurent expansion of $\tilde{H}_{T,L}(-s)$ in Eq. (69), beyond the singular term, correspond to higher order terms in the perturbative expansion of the twist-2 contribution. The next-to-leading order (NLO) contribution

originate from the constant term $b^{(1)}_{T,L}$. The obtained expression is of the form (72) without $(s+1)$ in the denominator. Thus, we immediately obtain

$$\Delta_b \, \sigma^{(\tau=2)}_{T,L}\Big|_{\rm NLO} \; = \; \frac{4\pi^2 b^{(1)}_{T,L}}{3\,Q^2} \; \alpha_s(CQ^2/4)\, g(x, CQ^2/4)\,, \tag{76}$$

which for the transverse polarization carries one power of the large logarithm $\log Q^2$ less than the leading term in $\Delta_a \sigma^{(\tau=2)}_T$. Notice that, as expected, for the longitudinal polarization the first non-vanishing twist-2 contribution enters at the NLO level. A similar procedure could also be applied to higher terms of the Laurent series, giving contributions with successively decreasing power of $\log Q^2$. Obviously, these higher order terms do not exhaust all the higher order QCD effects. They are parts of the QCD corrections to the twist-2 amplitude which come from inclusion of the quark transverse momentum in the quark box beyond the collinear limit

So far we have dealt with the singular part of $\tilde{\sigma}(x,s)$ at $s=-1$, generated by the first term in the perturbative part of the Glauber-Mueller series (58) proportional to the gluon distribution $g(x,\mu^2)$. The remaining terms of this series as well as the soft part $\tilde{\sigma}_{\rm soft}(x,s)$ are regular at $s=-1$. However, they contribute to twist-2 through the pole of $H_T(-s)$ at this point, giving

$$\Delta_c \sigma^{(\tau=2)}_T \; = \; -\frac{4a^{(1)}_T}{Q^2} \; \tilde{\sigma}^{(s=-1)}_{\rm reg}(x, s=-1)\,. \tag{77}$$

The function on the r.h.s is a sum of two pieces: the soft part, $\tilde{\sigma}_{\rm soft}(x, s=-1)$, and the Mellin transform of the regular part of the perturbative component, $\sigma_{\rm pert}(x,r) - \sigma^{(1)}_{\rm pert}(x,r)$, computed for $s=-1$. Thus

$$\tilde{\sigma}^{(s=-1)}_{\rm reg}(x, s=-1) \; = \int_0^{C/\mu_0^2} \frac{dr^2}{r^4} \left\{\sigma(x,r) - \sigma^{(1)}_{\rm pert}(x,r)\right\} \; + \; \tilde{\sigma}_{\rm soft}(x, s=-1)\,. \tag{78}$$

We summarize by displaying the most leading twist-2 contribution to the $\gamma^* p$ cross sections, obtained in the DGLAP improved saturation model (with $C=4$):

$$\sigma^{(\tau=2)}_T \; = \; \frac{8\pi^2 A_0}{9} \, \frac{1}{Q^2} \int_{\mu_0^2}^{Q^2} \frac{d\mu'^2}{\mu'^2} \; \alpha_s(\mu'^2)\, g(x,\mu'^2) \tag{79}$$

$$\sigma^{(\tau=2)}_L \; = \; \frac{8\pi^2 A_0}{9} \, \frac{1}{Q^2} \, \alpha_s(Q^2)\, g(x,Q^2)\,. \tag{80}$$

Notice the similarity concerning leading logarithms between the twist-2 contributions in the original GBW model, Eqs. (50) and (51), and the above formulae.

B. Twist-4 contributions

The formula for twist-4 is determined by the Mellin transform $\tilde{\sigma}^{(2)}_{\rm pert}(x,s)$ of the second term in Eq. (58) and the Laurent expansion of $\tilde{H}_{T,S}(-s)$ around $s=-2$:

$$\sigma^{(\tau=4)}_{T,L} \; = \int\limits_{-D^{(1)}_s} \frac{ds}{2\pi i} \left(\frac{Q^2}{4}\right)^s \left\{-\frac{\sigma_0}{2}\, \widetilde{\Omega^2_{\rm pert}}(x,s) \; + \; \tilde{\sigma}^{(s=-2)}_{\rm reg}(x,s)\right\} \left\{\frac{-a^{(2)}_{T,L}}{s+2} \; + \; b^{(2)}_{T,L} \; + \; \mathcal{O}(s+2)\right\} \tag{81}$$

where the integration contour envelopes the cut singularity with the branch point at $s=-2$ in which the function $\tilde{\sigma}^{(s=-2)}_{\rm reg}(x,s)$ is regular, see Fig. 6. The Laurent expansion coefficient are now given by

$$a^{(2)}_T = 0\,, \qquad a^{(2)}_L = -\tfrac{16}{15} A_0\,, \qquad b^{(2)}_T = -\tfrac{4}{5} A_0\,, \qquad b^{(2)}_L = \left(\tfrac{32}{15}\gamma_E - \tfrac{344}{225}\right) A_0\,. \tag{82}$$

The vanishing $a^{(2)}_T$ means that the leading logarithmic twist-4 contribution

$$\Delta_a \sigma^{\tau=4)}_T \; = \; \frac{\sigma_0\, a^{(2)}_T}{2} \int\limits_{-D^{(1)}_s} \frac{ds}{2\pi i} \left(\frac{Q^2}{4}\right)^s \frac{\widetilde{\Omega^2_{\rm pert}}(x,s)}{s+2}\,, \tag{83}$$

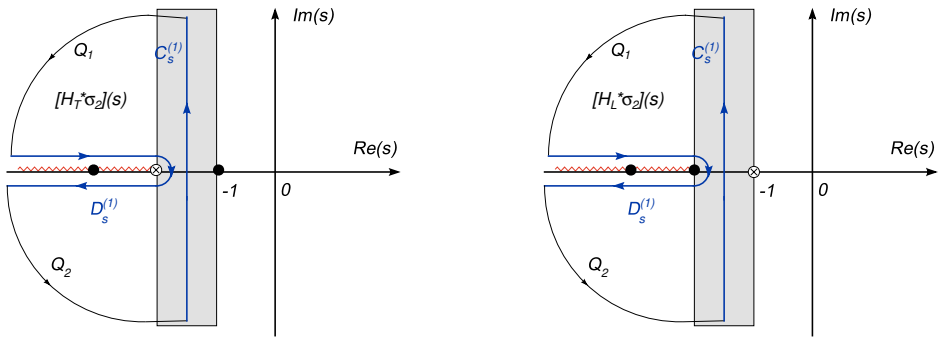

FIG. 6: The singularity structure in Mellin plane relevant for twist-4 transverse and longitudinal contributions together with the integration contours. The meaning of all symbols is as in Fig. 4, but the original contour, $\mathcal{C}_s$, is replaced by the shifted $\mathcal{C}_s^{(1)}$. The fundamental strip is also shifted.

vanishes for transverse photons. For the longitudinal polarization it can be found in a similar way as for twist-2, with the following result

$$\Delta_a \sigma_L^{(\tau=4)} \,=\, \frac{8\sigma_0 a_L^{(2)}}{Q^4}\left(\frac{\pi^2}{3\sigma_0}\right)^2 \left\{\int_{\mu_0^2}^{CQ^2/4} \frac{d\mu'^2}{\mu'^2}\left[\alpha_s(\mu'^2)\, g(x,\mu'^2)\right]^2 \,+\, S_L^{(4)}(x,\mu_0^2)\right\} \tag{84}$$

where the reminder is of non-perturbative origin and does not depend on Q^2,

$$S_L^{(4)}(x,\mu_0^2) \,=\, \frac{b_0^2}{\log\left(\frac{\mu_0^2}{\Lambda^2}\right)} \int \frac{d\omega}{2\pi i}\, x^{-\omega} \int \frac{d\omega'}{2\pi i}\, \frac{\tilde{g}_0(\omega')\,\tilde{g}_0(\omega-\omega')}{\frac{b_0}{2\pi}\tilde{P}_{gg}(\omega') + \frac{b_0}{2\pi}\tilde{P}_{gg}(\omega-\omega') - 1}\,. \tag{85}$$

The NLO correction to twist-4 comes from the constant term, $b_{T,L}^{(2)}$, in the Laurent expansion of $\tilde{H}_{T,L}(-s)$ around $s=-2$. It is straightforward to obtain

$$\Delta_b\, \sigma_{T,L}^{(\tau=4)}\Big|_{NLO} \,=\, -\frac{8\sigma_0 b_{T,L}^{(2)}}{Q^4}\left(\frac{\pi^2}{3\sigma_0}\right)^2 \left[\alpha_s(CQ^2/4)\, g(x,CQ^2/4)\right]^2\,, \tag{86}$$

which in the longitudinal case has one logarithm of Q^2 less then the leading contribution (84). As for twist-2, the higher terms in the Laurent expansion of $\tilde{H}_{T,L}(-s)$ give rise to yet higher order perturbative corrections.

Multiple scattering effects (with $n \geq 3$) and the soft contribution are important only for the longitudinal twist-4, $\sigma_L^{(\tau=4)}(x,Q^2)$. They are collected in

$$\Delta_c \sigma_L^{(\tau=4)} \,=\, -\frac{16 a_L^{(2)}}{Q^4}\left[\tilde{\sigma}_{\rm reg}^{(s=-2)}(x,s=-2) \,+\, \tilde{\sigma}_{\rm soft}(x,s=-2)\right] \tag{87}$$

where

$$\tilde{\sigma}_{\rm reg}^{(s=-2)}(x,s=-2) \,=\, \int_0^{C/\mu_0^2} \frac{dr^2}{r^6}\left[\sigma(x,r) - \sigma^{(1)}(x,r) - \sigma^{(2)}(x,r)\right]. \tag{88}$$

In summary, the following leading logarithmic structure is found for twist-4 (with $C=4$)

$$\sigma_T^{(\tau=4)} \,=\, \frac{32\pi^4 A_0}{45\,\sigma_0}\,\frac{1}{Q^4}\left[\alpha_s(Q^2)\, g(x,Q^2)\right]^2 \tag{89}$$

$$\sigma_L^{(\tau=4)} \,=\, -\frac{128\pi^4 A_0}{135\,\sigma_0}\,\frac{1}{Q^4}\int_{\mu_0^2}^{Q^2} \frac{d\mu'^2}{\mu'^2}\left[\alpha_s(\mu'^2)\, g(x,\mu'^2)\right]^2\,, \tag{90}$$

which should be compared to the results obtained in the original GBW saturation model, Eqs. (52) and (53). Notice the similarity in the sign and the leading logarithmic structure.

C. Discussion

The results (79),(80) and (89),(90) on the leading logarithmic behaviour of the twist-2 and twist-4 contributions are quite general. For the nucleon structure functions F_T and F_L they imply that the relative twist-4 correction to F_T is strongly suppressed w.r.t. the twist-2 contribution since the subleading twist-4 term in F_T appears only at the NLO. On the contrary, for F_L the leading twist term enters only at the NLO and the the twist-4 correction enters at the leading order. So, the relative twist-4 effects in F_L are expected to be enhanced. Note that both in the case of F_T and F_L, the twist-4 effects are enhanced w.r.t. the twist-2 contribution by an additional power of the gluon density $g(x,Q^2)$. At sufficiently small x, when the gluon density is large, this enhancement may compensate the twist-4 suppression w.r.t. the leading twist-2 contribution.

For the structure function $F_2 = F_T + F_L$ we expect small relative corrections from the higher twists because of the opposite sign of the terms proportional to $a_L^{(2)}$ and $b_{T,L}^{(2)}$. In fact, both $a_L^{(2)}$ and $b_{T,L}^{(2)}$ are negative. Thus it follows from (89) and (90) that the resulting LO twist-4 contribution to F_2 coming from F_L is positive and both the dominant (though NLO) term in F_T and the NLO correction to F_L are negative. This leads to partial cancellation between the twist-4 LO and NLO contributions to F_2 at moderate Q^2, which can be also viewed as a partial cancellation between the twist-4 corrections to F_L and F_T.

These conclusions about the importance of the higher twist corrections are expected to be quite general because they follow directly from the twist structure of the quark box and do not depend on the detailed form of the twist-4 gluon distribution. In fact, for a generic twist-4 gluon density $G_4(x,Q^2)$ (not necessarily proportional to $[g(x,Q^2)]^2$), the qualitative pattern of the computed twist-4 corrections emerges. This happens because independently of the detailed form of gluon density, the perturbative color dipole scattering cross section at twist-4 is proportional to $r^4\,\alpha_s(C/r^2)\,G_4(x,C/r^2)$. Using a generally valid relation: $\int (ds/2\pi i)\,x^{-s}\,\tilde f(s)/s = \int^x dx' f(x')$, one finds

$$\sigma_T^{(\tau=4)} \;\sim\; \frac{b_T^{(2)}}{Q^4}\,\alpha_s^2(Q^2)\,G_4(x,Q^2)\,, \tag{91}$$

and

$$\sigma_L^{(\tau=4)} \;\sim\; -\frac{a_L^{(2)}}{Q^4}\int^{Q^2}\frac{d\mu'^2}{\mu'^2}\,\alpha_s^2(\mu'^2)\,G_4(x,\mu'^2) \;+\; \frac{b_L^{(2)}}{Q^4}\,\alpha_s^2(Q^2)\,G_4(x,Q^2)\,. \tag{92}$$

This confirms that for twist-4 the pattern of cancellations in F_2 between F_L and F_T (or between LO and NLO terms) is indeed universal.

VII. TWIST DECOMPOSITION IN THE COORDINATE SPACE

The preceding analysis was carried out in the Mellin space. This representation is useful to understand the key features of the twist decomposition and match the DGLAP improved saturation model with QCD. However, in the explicit calculations of the twist composition of the $\gamma^* p$ cross sections we find it more convenient to use the coordinate representation. The main reason is that the multiple scattering contributions are represented as multiple convolutions in the Mellin space and as simple powers of $r^2\alpha_s(\mu^2)g(x,\mu^2)$ in the coordinate space. Thus, we shall construct an explicit prescription that facilitates the twist decomposition in the coordinate space. The obtained formula (99) is equivalent to its counterpart in the Mellin moment representation and it will be used to provide numerical estimates of the twist decomposition of the nucleon structure functions.

The singularity structure of the product $\tilde\sigma(x,s)\,\tilde H_{T,L}(-s,Q^2)$ is similar to the structure of $\tilde\sigma(x,s)$ except of the branch points of $\tilde\sigma(x,s)$ which are strengthened by the poles of $\tilde H_{T,L}(-s,Q^2)$. In what follows, we shall isolate the contributions of the singularities emerging at $s=-1,-2,\ldots$ and link them with the twist contributions $\tau=2,4,\ldots$, respectively Let us define two sets of functions,

$$\sigma^{(n)}(x,r) = \sigma(x,r) \;-\; \sigma_0\sum_{k=1}^{n}\frac{(-1)^k}{k!}\,\Omega^k(x,r^2) \tag{93}$$

and after introducing $\hat r = rQ$

$$H_{T,L}^{(n)}(\hat r) = H_{T,L}(\hat r) \;-\; \sum_{k=1}^{n}\frac{h_{T,L}^{(k)}}{(\hat r)^{2k}} \tag{94}$$

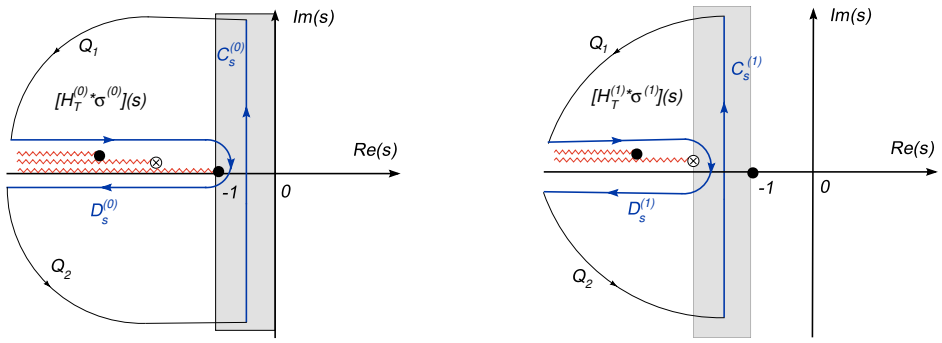

FIG. 7: The singularity structure of $\tilde{\sigma}^{(0)}(x,s)\tilde{H}_T(-s,Q^2)$ and $\tilde{\sigma}^{(1)}(x,s)\tilde{H}_T(-s,Q^2)$, and the integration contours in the complex s-plane. The meaning of all symbols is as in Fig. 4 – additionally, pieces of the closed integration contour are shown: $\mathcal{C}_s^{(1)}$, $\mathcal{D}_s^{(0)}$, $\mathcal{D}_s^{(1)}$, etc.

where $h_{T,L}^{(k)}$ are the coefficients of the asymptotic expansion of $H_{T,L}(\hat{r})$, see Eq. (39). Additionally, $\sigma^{(0)} = \sigma$ and $H_{T,L}^{(0)} = H_{T,L}$. We see that $\sigma^{(n)}$ describes the contribution to the dipole cross section of $(n+1)$ and more scatterings and $H_{T,L}^{(n)}$ gives the contribution to the photon wave function from the poles of twist $\tau = 2(n+1)$ and higher. The new functions have the following asymptotics at small and large values of r (modulo logarithms):

$$\sigma^{(n)}(x,r) \;\sim\; \begin{cases} (r^2)^{n+1} & \text{for } r \to 0 \\ (r^2)^n & \text{for } r \to \infty \end{cases} \tag{95}$$

and

$$H_{T,L}^{(n)}(\hat{r}) \;\sim\; \begin{cases} 1/\hat{r}^{2n} & \text{for } r \to 0 \\ 1/\hat{r}^{2(n+1)} & \text{for } r \to \infty\,. \end{cases} \tag{96}$$

Now, it is easy to prove that $\sigma^{(n)}(x,r)$ and $H_{T,L}^{(n)}(\hat{r})$ have Mellin transforms, $\tilde{\sigma}^{(n)}(x,s)$ and $\tilde{H}_{T,L}^{(n)}(-s,Q^2)$, with the fundamental strip:

$$-(n+1) < \mathrm{Re}\, s < -n\,. \tag{97}$$

It is moved to the left by n units with respect to the fundamental strip given by Eq. (24).

The singularities of the Mellin transform $\tilde{\sigma}^{(n)}(x,s)$ emerging at the branch point to the left of its fundamental strip are the same as the corresponding singularities of the functions: $\tilde{\sigma}^{(0)}(x,s)$, $\tilde{\sigma}^{(1)}(x,s), \ldots, \tilde{\sigma}^{(n-1)}(x,s)$. The functions $H_{T,L}^{(n)}(\hat{r})$ are shifted with respect to $H_{T,L}(\hat{r})$ by a finite power series in $1/\hat{r}^2$, so their Mellin transforms are identical and equal to the Mellin transform $\tilde{H}_{T,L}(s,Q^2)$ for all n. The series subtraction results only in the already discussed shift in the position of the fundamental Mellin strip. Therefore, the difference

$$\Delta^{(n)}[\sigma H_{T,L}](x,Q^2) \;=\; \int_{\mathcal{C}_s^{(n-1)}} \frac{ds}{2\pi i}\, \tilde{\sigma}^{(n-1)}(x,s)\, \tilde{H}_{T,L}^{(n-1)}(-s,Q^2) \;-\; \int_{\mathcal{C}_s^{(n)}} \frac{ds}{2\pi i}\, \tilde{\sigma}^{(n)}(x,s)\, \tilde{H}_{T,L}^{(n)}(-s,Q^2) \tag{98}$$

defines the contribution of the n-th singularity (i.e. the cut discontinuity with the branch point at $s=-n$) to the integral in Eq. (21), see Fig. 7 for illustration. In our analysis we identify this contribution with the $\tau = 2n$ twist component of $\sigma_{T,L}^{\gamma^* p}$.

The Mellin integrals in Eq. (98) may be expressed in the coordinate space to give a formula that facilitates a direct determination of all twists in the coordinate representation:

$$\sigma_{T,L}^{(2n)}(x,Q^2) \;=\; \int_0^\infty \frac{dr^2}{r^2} \left\{ \sigma^{(n-1)}(x,r)\, H_{T,L}^{(n-1)}(rQ) \;-\; \sigma^{(n)}(x,r)\, H_{T,L}^{(n)}(rQ) \right\}. \tag{99}$$

Clearly, the twist decomposition would be complete and

$$\sum_{n=1}^{\infty} \sigma_{T,L}^{(\tau=2n)} \;=\; \sigma_{T,L}^{\gamma^* p} \tag{100}$$

provided that the infinite summation of $\Delta^{(n)}[\sigma H_{T,L}](x,Q^2)$ is convergent[1].

The prescription given by Eq. (99) may be also applied to the original GBW dipole cross section which Mellin transform has a series of isolated poles at $s=-n$ instead of the series of cut singularities. In this case, in Eq. (93) a polynomial is subtracted and the Mellin transform of $\sigma^{(n)}(x,r)$ is identical to $\tilde{\sigma}(x,s)$ given by Eq. (45). Therefore, formulae (98) and (99) may also be applied to extract the contribution from all singularities of $\tilde{\sigma}(x,s)H_{T,L}(-s,Q^2)$ to give the twist expansion in the case of the GBW dipole cross section. An explicit numerical check showed that the expansion obtained using prescription (99) agrees with the analytic results in [11].

VIII. HEAVY QUARKS

So far we studied the massless quark contribution. Within the k_T-factorization approach it is straightforward to study also the case with a non-zero quark mass. In particular, the Mellin transforms of the photon wave functions squared with $m_f \neq 0$, which generalize expressions (A9) and (A10), are known [12]. We shall denote them by $\tilde{H}_{T,L}(s,Q^2,m_f^2)$. The contribution of a heavy quark to the $\gamma^* p$ cross section may be obtained using the Parseval formula (21) in which the replacement $\tilde{H}_{T,L}(-s,Q^2) \to \tilde{H}_{T,L}(-s,Q^2,m_f^2)$ is made. For $\mathrm{Re}\, s > 0$, the functions $\tilde{H}_{T,L}(s,Q^2,m_f^2)$ are regular in s. Therefore, the s-singularity structure of the integrand $\tilde{\sigma}(x,s)\tilde{H}_{T,L}(-s,Q^2,m_f^2)$ in (21) is determined by the singularity structure of $\tilde{\sigma}(x,s)$. Hence, for heavy quarks the twist-τ component is determined by the n-fold scattering component of the dipole cross-section,

$$\sigma_{T,L}^{(\tau=2n)}(x,Q^2,m_f) \;=\; \int_0^\infty \frac{dr^2}{r^2}\, H_{T,L}(r^2,Q^2,m_f^2)\, \sigma_n(x,r^2) \tag{101}$$

where $\sigma_n(x,r^2) = \sigma_0(-1)^{n+1}\,\Omega^n(x,r^2)/n!$. Note that for heavy quarks with $m_f^2 \gg \mu_0^2$, the integration in (101) does not lead to any infra-red divergences since the photon wave function provides an exponential cut-off proportional to $\exp(-r m_f)$ for the r^2 integration. This was not the case for the light quarks, when $m_f^2 \ll \mu_0^2$, for which formula (101) cannot be applied.

IX. PHENOMENOLOGICAL RESULTS AND CONSEQUENCES

In this section the obtained estimates are presented for the higher twist effects in F_T, F_L and F_2, and also, separately, for the charm quark components of F_T, F_L and F_2. Additionally, we discuss the phenomenological consequences of our findings for the measurements at the LHC. We performed an explicit numerical evaluation of higher twist components of the proton structure functions in the DGLAP improved saturation model, defined by Eqs. (42)–(43) with the evolution scale given by Eq. (54):

$$\mu^2 \;=\; \begin{cases} C/r^2 & \text{for} \quad r^2 < C/\mu_0^2 \\ \mu_0^2 & \text{for} \quad r^2 \geq C/\mu_0^2 \,. \end{cases}$$

Furthermore, we compared the results to those obtained in [11] within the GBW model [12] without the DGLAP evolution.

The parameters of the DGLAP improved saturation model were fitted to describe all HERA data on F_2 at $x < 0.01$. In the model we took into account three massless quark flavors and the massive charmed quark with $m_c = 1.3$ GeV. The gluon density at the input scale $Q_0^2 = 1$ GeV^2 was assumed to take the form

$$xg(x,Q_0^2) = A_g\, x^{-\lambda}\,(1-x)^{5.6}\,. \tag{102}$$

The parameters obtained from the best fit with $\chi^2 = 0.94$/d.o.f are the following:

$$C = 0.55\,, \qquad \mu_0^2 = 1.62\,, \qquad A_g = 1.07\,, \qquad \lambda = 0.14\,, \qquad \sigma_0 = 22 \text{ mb}\,. \tag{103}$$

---

[1] In fact the series in not convergent; the expression was obtained assuming the validity of the asymptotic $H_{T,L}(rQ)$ expansion for large rQ down to $rQ = 0$. Therefore, the obtained series is asymptotic.

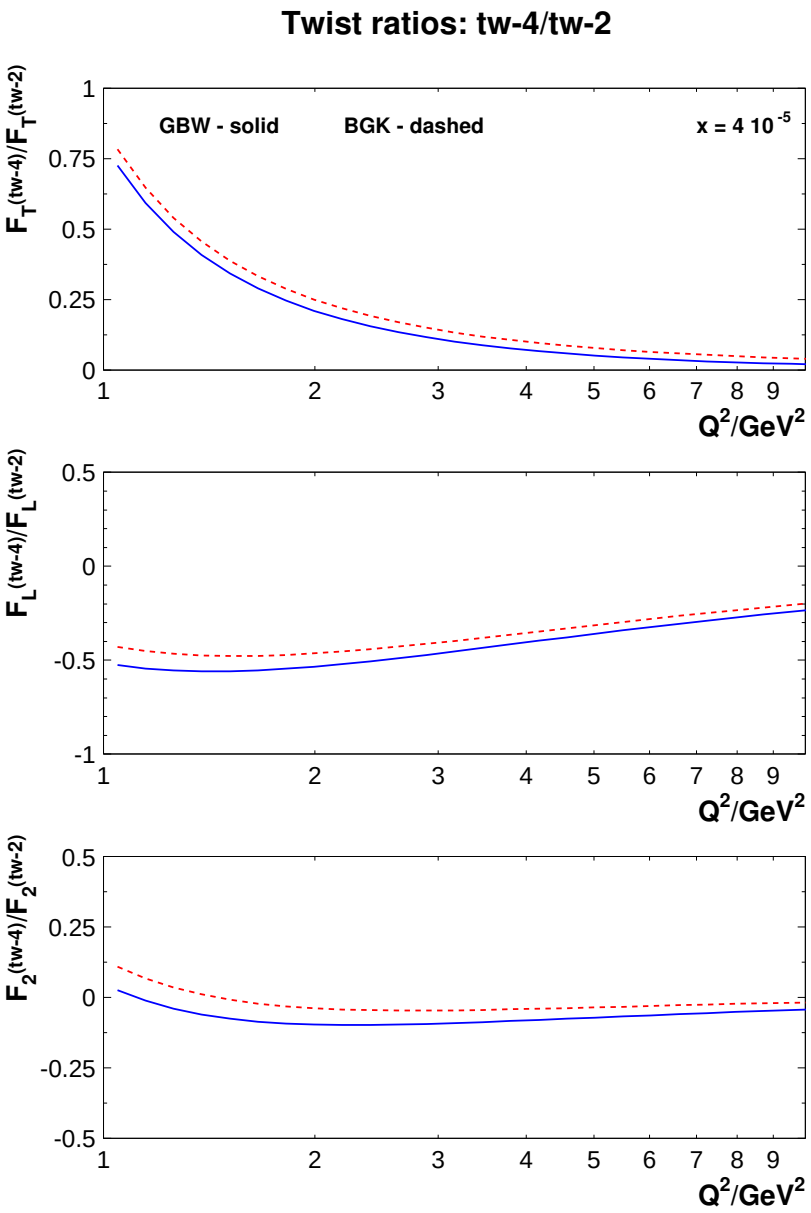

FIG. 8: The ratio of twist-4 to twist-2 components of F_T, F_L and F_2 at $x = 4 \cdot 10^{-5}$ in the GBW model with charm (continuous lines) and in the DGLAP improved saturation model (dashed lines).

A. Structure functions

The obtained relative twist-4 corrections (with respect to the twist-2 ones) to the structure functions F_T, F_L and F_2 are displayed in Fig. 8, as a function of Q^2, for $x = 4 \cdot 10^{-5}$ (for this value the saturation scale $Q_s(x) = 1$ GeV in the GBW model with charm). The continuous curves obtained in [11] correspond to the GBW model with charm quarks [12], and the dashed ones are obtained in the DGLAP improved saturation model (BGK) [15] with the parameters given above. The differences between the GBW model and the BGK models are visible, but rather small. The qualitative picture is fully consistent between the models and agrees very well with the results of the analytic analysis outlined in Sec. VI. Thus, the higher twist corrections are strongest in F_L, and much weaker in F_T. In F_2 there occurs a rather fine cancellation between the twist-4 contributions to F_T and F_L, at all Q^2, down to 1 GeV^2. Although an effect of this kind was expected, it still remains somewhat surprising that this cancellation works so well.

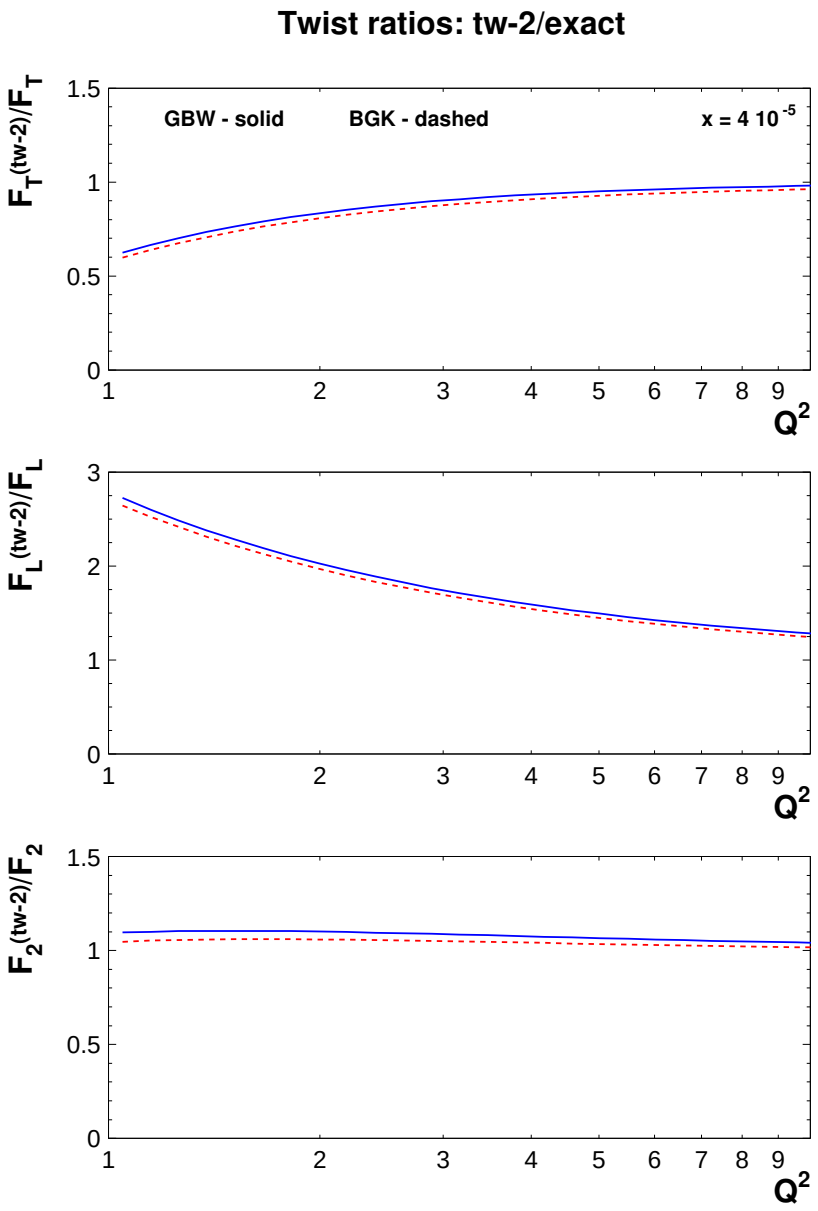

FIG. 9: The ratio of the twist-2 component to the full light quark result of the model for F_T, F_L and F_2 at $x = 4 \cdot 10^{-5}$ in the GBW model with charm (continuous lines) and in the DGLAP improved saturation model (dashed lines).

We also show in Fig. 9 the ratio of the twist-2 component to the full dipole model result for F_T, F_L and F_2. The full result incorporates the resummed contributions of all twists. On the qualitative level, the effect of all higher twists shown in Fig. 9 are similar to the effect of twist-4 in Fig. 8, indicating that the higher twist corrections are driven by the twist-4 contribution down to $Q^2 = 1$ GeV^2. It is remarkable, that the cancellation of the higher twist effects in F_2 occurs also in the all-twist result. Clearly, the results shown in Fig. 9 indicate that at lower Q^2, the conventional twist-2 calculations underestimate the value of F_T, significantly overestimate the value of F_L and slightly overestimate the value of F_2.

One should stress, that the theoretical conclusions about the strength of the higher twist corrections, related to the powers of α_s, are only valid in the perturbative range, where α_s is small. They are therefore, well justified for Q^2 above, say, 5 GeV^2. In that region, indeed, the difference between higher twists in F_L and F_T is quite pronounced. At lower Q^2, where α_s is not small, the differences in powers of α_s should not lead to quantitatively distinct results in

F_T and F_L. Indeed, at $Q^2 = 1$ GeV^2, the relative twist-4 corrections to F_T and F_L are 30% and 50% correspondingly, that is they do not differ very much.

B. Charm contribution

The DIS cross-section at small-x and a moderate Q^2 receives significant contribution from the charmed quark. The contribution of the bottom quark may be safely neglected due to its small charge $e_b = 1/3$ and its large mass. For the region of interest, $Q^2 \sim 10$ GeV^2, the mass, m_c, of the charmed quark cannot be neglected, as $Q^2 \sim 4m_c^2$. Therefore, our extraction of the higher twist effects in charm structure functions F_T^c and F_L^c is based on the results of Sec. VIII. The results for higher twist effects in the charm structure functions F_T^c and F_L^c are shown in Fig. 10. Displayed are the twist-2 and twist-4 components and the all-twist result. In contrast with the case of the light quarks, the higher twist effects introduce negative corrections both in F_T^c and in F_L^c, and the magnitude of the ratio of twist-4 to twist-2 contributions is similar in both cases and reaches a few percent. Consequently, the effect of higher twists in F_2^c is similar.

C. Comparison with F_L data

Recently, new measurements were performed of the proton F_L structure function in a wide kinematic range [16]. The measurements probe F_L for correlated (x, Q^2) pairs down to $x = 5.9{\cdot}10^{-5}$ and $Q^2 = 1.8\,\mathrm{GeV}^2$, see Fig. 11. The data in the lowest range of x are particularly interesting, as in this region, the leading twist, fixed order DGLAP calculations face intrinsic problems [32, 33]. Specifically, in that region, the convergence of the subsequent F_L approximations within perturbative expansions is rather poor, up to the next-to-next-leading order (NNLO) approximation [33]. In addition, at very small x and low Q^2, the estimated F_L becomes negative, violating the fundamental condition of positivity [33]. This indicates that the DGLAP treatment in this region has to be improved. In what follows, we shall present the comparison of the new F_L data with the dipole model results, and we shall shortly compare our approach with another successful approach to F_2 and F_L, based on the leading twist DGLAP scheme, improved by a small x resummation [32].

In Fig. 11 we show the comparison of our results with the preliminary data on F_L from the H1 collaboration. In the top of the plot, the values of x are indicated for each data point. Note that the experimental data points show strong correlation between the values of Q^2 and x. Thus, small Q^2 values are measured for smaller values of x. The solid curve represents the all twist result from the DGLAP improved saturation model applied in this paper, while the dashed line shows the twist-2 contribution within this model. The difference between the two curves comes from the negative higher twist terms, with a dominant contribution of twist-4. The description of the data provided by the model is good, both for the twist-2 approximation and the all-twist result. We stress, that all the model parameters are fixed by the fit to F_2 data and no new parameters are introduced in the description of F_L.

Clearly, the low Q^2 region of the plot, where x is also small, is highly sensitive to higher twist effects. In particular, for the lowest measured values of (x, Q^2), the twist-2 contribution is already about two times larger then the exact result. Unfortunately, the current experimental errors are sizable and no evidence for higher twist effects can be drawn from the measurements, yet. We stress, however, that F_L at small x and Q^2 should be an excellent observable to find such effects, provided that the experimental errors may be further reduced.

The defects of the fixed order DGLAP description of F_L at small x and Q^2 were shown to be partially cured by including into the DGLAP framework a resummation of small x corrections, enhanced by powers of $\log x$. The resummation, proposed by Thorne and White (TW) [32], absorbs the NLL BFKL effects at the leading twist into the NLO DGLAP evolution. In the currently relevant kinematic range, the description of F_L based on the TW approach is remarkably similar [33] to the one obtained within a saturation model with the impact parameter dependence (the, so called, b-Sat model) [34]. In addition, the b-Sat model results for F_L agree well with the results of this paper. The TW scheme provides a good description of the existing F_L data. The F_L at small x and Q^2 following from the saturation models is significantly lower than the corresponding TW result, but the differences are not pronounced enough to permit a discrimination between the approaches with the present data. Let us, however, stress, that the asymptotic $x \to 0$ (or $Q^2 \to 0$) behaviour of the structure functions should be different in approaches consistent with unitarity constraints, (as e.g. the saturation models), and the leading twist approach. In the former case, F_L should vanish in the limit, while in the latter case it should remain non-zero. Thus, one expects, that the leading twist approach should be insufficient at a very low x and fixed Q^2, and that the inclusion of higher twist effects should be necessary in that limit.

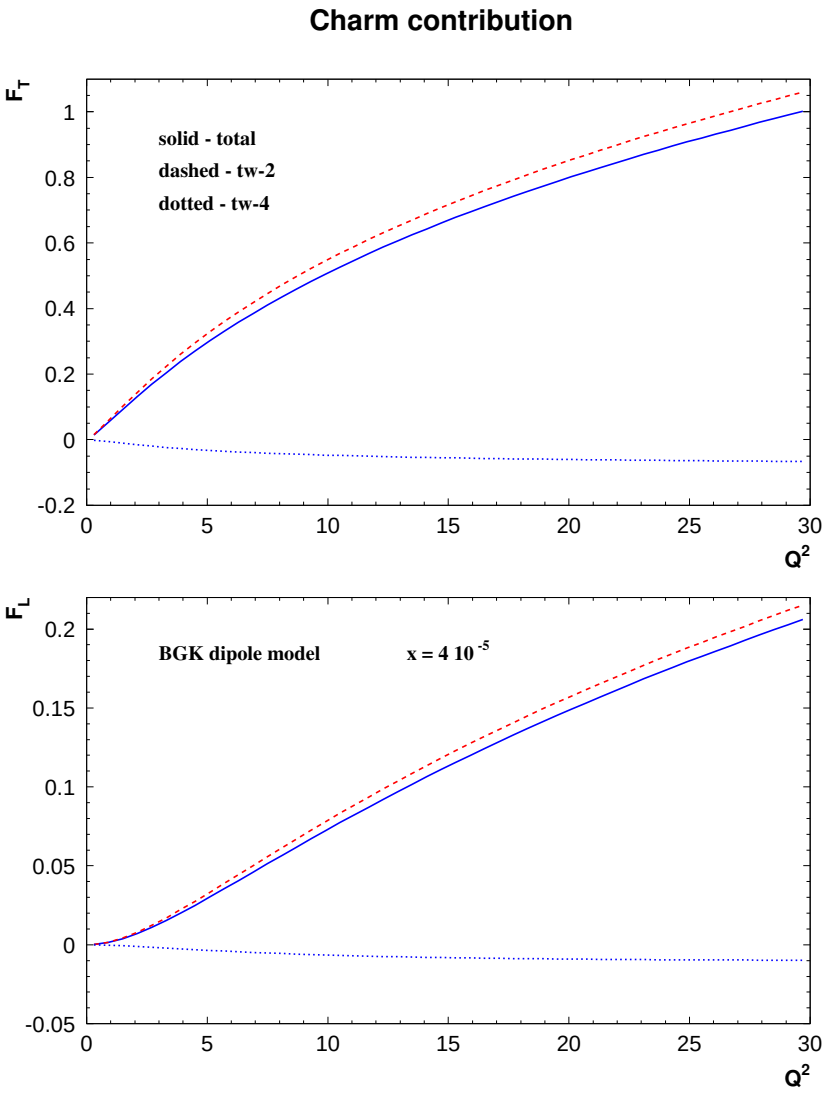

FIG. 10: Charm contribution to F_T and F_L at $x = 4 \cdot 10^{-5}$ in the DGLAP improved saturation model. Shown are the contributions of the twist-2 component (dashed lines), the twist-4 component (dotted lines) and the full result (continuous lines).

D. Discussion and implications for the LHC

The analysis performed in this paper shows that the importance of the higher twist corrections may essentially depend on the process and the probe. In particular, higher twist effect in the structure function F_2 are strongly suppressed due to rather fine cancellations between F_T and F_L. Such cancellations are not expected to occur in a generic case. For instance, the higher twist effect in F_L are enhanced. Thus far, parton density functions (pdfs) in DIS were fitted mostly to the F_2 data. Due to small higher twist effects in F_2, one expects that the suppressed higher twist contributions should not affect the quality of the determination of pdfs. This is, certainly, a good news. The estimated correction due to higher twist effects in F_L at small x and a moderate Q^2 is, however, much larger, and this correction should be taken into account when including the F_L data into fits of pdfs.

The example of F_2 and F_L in the DIS shows that the multiple scattering (higher twist) effects are probed in various ways, depending on the observable. Similar differences in the magnitude of higher twist effects in various observables may occur in the hadronic collisions, e.g. in pp collisions at the LHC. In particular, cancellations present in F_2 is not expected for the bulk of LHC observables probing the gluon distributions at small-x. Thus, in general, the relative

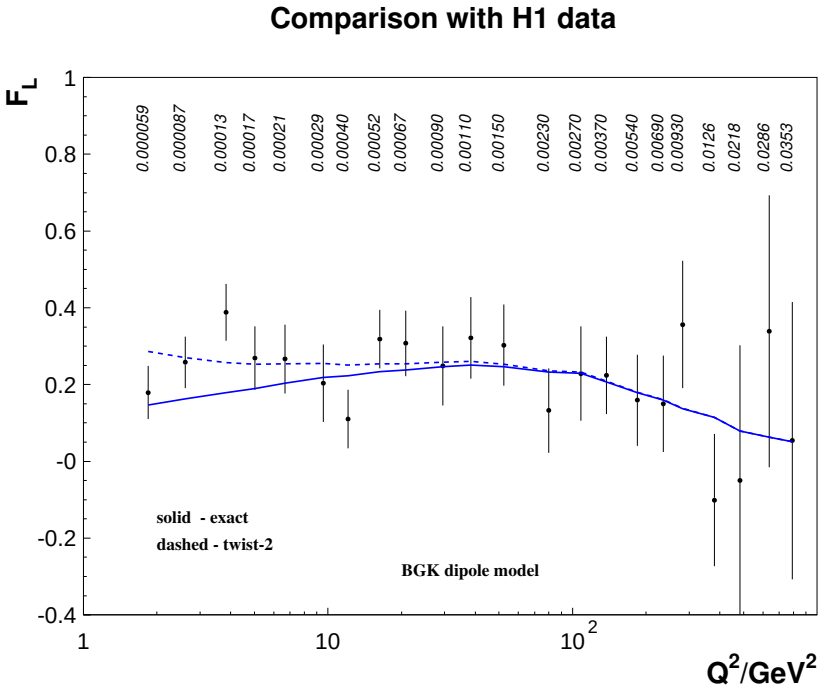

FIG. 11: Comparison of the DGLAP improved saturation model with the preliminary H1 on F_L [16]. The solid line is the all-twist result while the dashed line shows the twist-2 contribution. The value of x is indicated for each data point.

effects of higher twists at the LHC should be larger than they are in F_2. As an example, let us give the case of the forward Drell-Yan process, that can be effectively described using the dipole formulation [35]. At LHC-b, the Drell-Yan process may be probed at moderate $Q^2 \sim 10$ GeV^2 and $x \sim 10^{-6}$, what should provide a gold-plated probe of the gluon density at small x. However, the higher twists effects may be quite strong there. In particular, let us invoke an example of the Lam–Tung relation [36] that holds for angular distribution of Drell-Yan lepton pairs. According to this relation, the twist-2 contribution to one of the angular components of the dilepton distribution vanishes in the leading logarithmic approximation. Therefore, higher twist effects in this component should be enhanced, in analogy to the case F_L [36, 37]. Thus, given the low values of x and Q^2, that can be reached in the measurements in LHC-b, the violations of Lam-Tung relation should provide a sensitive probe of the higher twist gluonic operators at small x. On the other hand, the higher twist effect may be also large in the total cross-section of the forward Drell-Yan process. In that case, a determination of gluon density at small x, based on the leading twist contribution alone would be inaccurate, and the higher twist contributions should be taken into account. Besides that, the higher twist effects may be larger in processes with gluons, like e.g. the forward gluonic jet productions, where the multiple scattering of the gluon is enhanced by its color charge, as compared to the quark rescattering in the DIS case. In such processes, we do not expect that any cancellations of rescattering effects should occur, of the type found in F_2.

X. CONCLUSIONS

In this paper the leading higher twist contributions to proton structure functions, F_2, F_T and F_L, at small Bjorken x and moderate Q^2 were analyzed. The problem was analyzed theoretically confronting two different approaches. In the fist approach, we focused on a subset of QCD diagrams describing contributions of quasipartonic gluon operators, that should dominate the higher twist effects in the deeply inelastic scattering at small x. We demonstrated, that this subclass of the diagrams, at the leading logarithmic approximations and in the large N_c leads to a picture consistent with the DGLAP improved saturation model. In contrast, we considered also the problem of higher twists in the Balitsky-Kovchegov framework, in which, the BFKL Pomeron fan diagram are resummed. In this approach, higher twist contributions coming from the fan diagrams vanish in the leading $\log Q^2$ approximation.

The pattern of the most important twist-2 and twist-4 contributions to F_2, F_T and F_L is determined by the properties

of the quark loop through which the virtual photon interacts with the gluonic field of the proton. Therefore, it is universal and its key features should not depend on the model details. Those features are: (i) the twist-4 correction to F_T enters only at the NLO, and so, the twist-4 correction to F_T is suppressed; (ii) the twist-2 contribution to F_L enters at NLO, and the LO twist-4 term in F_L is relatively enhanced and more important; (iii) the relative sign of twist-4 corrections to F_T and F_L is opposite, and the higher twist effects partially cancel in $F_2 = F_T + F_L$. These general conclusions were then confirmed by a quantitative phenomenological analysis.

We performed a numerical twist analysis of the DIS cross-sections at small-x within the DGLAP improved saturation model. In order to carry out a quantitative estimate of the higher twist effects in the structure functions, we proposed a method allowing for a direct, numerical twist decomposition of the saturation model cross sections. The method was then applied to the DGLAP improved saturation model, fitted to the HERA F_2 data. Contributions of twist-2, twist-4 and all twists to F_2, F_T and F_L were then extracted. We found a strikingly good cancellation of the higher twist effects in F_2, for which, at $x = 3 \cdot 10^{-4}$, the relative correction from higher twists is found to be at a few percent level down to $Q^2 = 1$ GeV^2. The higher twist corrections to F_T were found to be moderate, below 10% for $Q^2 > 3$ GeV^2 at $x = 3 \cdot 10^{-4}$. On the other hand, the twist-4 correction in F_L was found to be large, about 50%, at $Q^2 = 1$ GeV^2, and still sizeable, about 20%, at $Q^2 = 10$ GeV^2. Therefore, whereas the leading twist analyses of F_2 are fully justified, one should include the higher twist effects in analyses of the F_L data at small x and moderate Q^2. We also found that the saturation model description of the recent F_L measurements at small x and low Q^2 is good. Unfortunately, the data are not precise enough to prove that the inclusion of higher twist corrections improves the description of the data.

Finally, some implications were discussed of the results for analyzes of the LHC data. In particular, we stressed a strong process-dependence of the higher twist contributions, exemplified before by the striking differences between F_2 and F_L. It follows from our analysis, that F_2 is protected by cancellations from the higher twist effects, and such cancellations are not expected to be generic. Therefore, the higher twist effects in some LHC observables may be much stronger that they are in F_2. Thus, it is crucial to estimate higher twist effects when attempting a precise determination of parton densities in LHC measurements at small x and moderate Q^2, like e.g. in the forward Drell-Yan process at low Q^2, or in the forward jet production.

Acknowledgements

LM acknowledges the support of the DFG grant SFB 676. This work is partially supported by the grant MNiSW no. N202 249235.

APPENDIX A: MELLIN TRANSFORMS OF $H_{T,L}$

Let us compute the Mellin transform of $H_T(rQ)$ given by Eq. (25)

$$\tilde{H}_T(s,Q^2) \;=\; \int_0^\infty dr^2\,(r^2)^{s-1}\,H_T(rQ)\,. \tag{A1}$$

Substituting Eq. (25) we obtain

$$\tilde{H}_T(s,Q^2) \;=\; \left(\frac{Q^2}{4}\right)^{-s}\,\tilde{H}_T(s) \tag{A2}$$

where

$$\tilde{H}_T(s) = 4^{-s}A_0\int_0^1 dz\,[z^2+(1-z)^2]\,z(1-z)\int_0^\infty d\hat{r}^2\,(\hat{r}^2)^s\,K_1^2(\sqrt{z(1-z)}\,\hat{r})\,. \tag{A3}$$

with $\hat{r} = rQ$. Changing the variable, $y^2 = z(1-z)\hat{r}^2$, we find

$$\tilde{H}_T(s) = 4^{-s}A_0\int_0^1 dz\,\frac{z^2+(1-z)^2}{z^s(1-z)^s}\int_0^\infty dy^2\,(y^2)^s\,K_1^2(y)\,. \tag{A4}$$

The integral over z equals

$$I_z \equiv \int_0^1 dz\,\frac{z^2+(1-z)^2}{z^s(1-z)^s} = 2\int_0^1 dz\,z^{2-s}(1-z)^{-s} = 2\,\frac{\Gamma(3-s)\Gamma(1-s)}{\Gamma(4-2s)} \tag{A5}$$

where we used the definition of the Euler beta function. The gamma function in the denominator can be written as

$$\Gamma(2(2-s)) = \frac{2^{2(2-s)-1}}{\sqrt{\pi}}\,\Gamma(2-s)\Gamma(2-s+1/2) \tag{A6}$$

and from this we have

$$I_z = \frac{\sqrt{\pi}}{4^{1-s}}\,\frac{\Gamma(1-s)\Gamma(3-s)}{\Gamma(2-s)\Gamma(5/2-s)}\,. \tag{A7}$$

The integral over y^2 in Eq. (A4) equals

$$\int_0^\infty dy^2\,(y^2)^s\,K_1^2(y) = 2\int_0^\infty dy\,y^{2s+1}\,K_1^2(y) = 2\,\frac{\sqrt{\pi}}{4}\,\frac{\Gamma(2+s)\Gamma(1+s)\Gamma(s)}{\Gamma(3/2+s)}\,. \tag{A8}$$

Thus, we finally find

$$\tilde{H}_T(s) \;=\; \frac{A_0\,\pi}{8}\,\frac{\Gamma(2+s)\,\Gamma(1+s)\,\Gamma(s)\,\Gamma(1-s)\,\Gamma(3-s)}{\Gamma(3/2+s)\,\Gamma(2-s)\,\Gamma(5/2-s)}\,. \tag{A9}$$

A similar calculation allows to compute the Mellin transform

$$\tilde{H}_L(s) \;=\; \frac{A_0\,\pi}{4}\,\frac{(\Gamma(1+s))^3\,\Gamma(2-s)}{\Gamma(3/2+s)\,\Gamma(5/2-s)} \tag{A10}$$

APPENDIX B: EVOLUTION OF THE GLUON DENSITY

The gluon density used in our analysis, $g(x,\mu^2) \equiv xG(x,\mu^2)$, obeys the following leading logarithmic DGLAP evolution equation:

$$\mu^2\frac{\partial g(x,\mu^2)}{\partial\mu^2} \;=\; \frac{\alpha_s(\mu^2)}{2\pi}\int_x^1 dz\,P_{gg}(z)\,g\left(\frac{x}{z},\mu^2\right) \tag{B1}$$

where the contribution from quarks is neglected and the gluon splitting function P_{gg} takes the form,

$$P_{gg}(z) = 6\left[\frac{1-z}{z} + z(1-z) + \frac{z}{(1-z)_+} + \frac{11}{12}\delta(1-z)\right] - \frac{n_f}{3}\delta(1-z) \tag{B2}$$

and the one loop strong coupling is given by

$$\alpha_s(\mu^2) = \frac{b_0}{\log(\mu^2/\Lambda^2)} \tag{B3}$$

with $b_0 = 12\pi/(33-2n_f)$. This equation may be solved in the double Mellin moment space,

$$g(x,\mu^2) = \int\frac{d\omega}{2\pi i}\,x^{-\omega}\int\frac{d\gamma}{2\pi i}\,\tilde{g}(\omega,\gamma)\left(\frac{\mu^2}{\Lambda^2}\right)^\gamma \tag{B4}$$

where $\tilde{g}(\omega,\gamma)$ obeys the following equation

$$-\frac{\partial}{\partial\gamma}\left\{\gamma\tilde{g}(\omega,\gamma)\right\} = \frac{b_0}{2\pi}\,\tilde{P}_{gg}(\omega)\,\tilde{g}(\omega,\gamma) \tag{B5}$$

and the splitting kernel in the Mellin representation, $\tilde{P}_{gg}(\omega)$, is given by

$$\tilde{P}_{gg}(\omega) = \int_0^1 dz\,z^\omega P_{gg}(z) = 6\left[\frac{1}{\omega} - \frac{1}{\omega+1} + \frac{1}{\omega+2} - \frac{1}{\omega+3} - \gamma_E - \psi(\omega+2)\right] + \frac{33-2n_f}{6}\,. \tag{B6}$$

The general solution to Eq. (B5) reads

$$\tilde{g}(\omega,\gamma) \;=\; \tilde{g}_0(\omega)\,\gamma^{-1-\frac{b_0}{2\pi}\bar{P}_{gg}(\omega)} \tag{B7}$$

where $\tilde{g}_0(\omega)$ is an arbitrary function which may be fixed using an initial condition. Thus, the solution expressed in terms of the original variables (x, μ^2) is given by

$$g(x,\mu^2) \;=\; \int \frac{d\omega}{2\pi i}\, x^{-\omega}\, \tilde{g}_0(\omega) \int \frac{d\gamma}{2\pi i}\, \gamma^{-1-\frac{b_0}{2\pi}\bar{P}_{gg}(\omega)} \left(\frac{\mu^2}{\Lambda^2}\right)^{\gamma}. \tag{B8}$$

The contour integral over γ may be performed for all $\mu^2 > \Lambda^2$ after the integration contour is deformed to envelope the cut along the negative real half-axis. We find

$$g(x,\mu^2) \;=\; \int \frac{d\omega}{2\pi i}\, x^{-\omega}\, \tilde{g}(\omega,\mu^2) \tag{B9}$$

where

$$\tilde{g}(\omega,\mu^2) \;=\; \frac{\tilde{g}_0(\omega)}{\Gamma\left(1+\frac{b_0}{2\pi}\tilde{P}_{gg}(\omega)\right)} \quad \left[\log\left(\frac{\mu^2}{\Lambda^2}\right)\right]^{\frac{b_0}{2\pi}\bar{P}_{gg}(\omega)}. \tag{B10}$$

The initial condition for the DGLAP equation at some scale $\mu_0^2 \gg \Lambda^2$ is given by its Mellin transform $\tilde{g}(\omega, \mu_0^2)$. Thus, writing (B10) for $\mu^2 = \mu_0^2$, we obtain

$$\tilde{g}_0(\omega) \;=\; \tilde{g}(\omega,\mu_0^2)\, \Gamma\left(1+\frac{b_0}{2\pi}\tilde{P}_{gg}(\omega)\right) \quad \left[\log\left(\frac{\mu_0^2}{\Lambda^2}\right)\right]^{-\frac{b_0}{2\pi}\bar{P}_{gg}(\omega)}, \tag{B11}$$

which in turn, after the substitution to (B9), leads to the well known form

$$g(x,\mu^2) = \int \frac{d\omega}{2\pi i}\, x^{-\omega}\, \tilde{g}(\omega,\mu_0^2) \left[\frac{\log(\mu^2/\Lambda^2)}{\log(\mu_0^2/\Lambda^2)}\right]^{\frac{b_0}{2\pi}\bar{P}_{gg}(\omega)}. \tag{B12}$$

We also need the double Mellin representation of the product $\alpha_s(\mu^2)g(x,\mu^2)$. In the mixed (ω,μ^2) representation the DGLAP equation (B1) reads

$$\mu^2 \frac{\partial \tilde{g}(\omega,\mu^2)}{\partial \mu^2} \;=\; \frac{\tilde{P}_{gg}(\omega)}{2\pi}\, \alpha_s(\mu^2)\, \tilde{g}(\omega,\mu^2)\,. \tag{B13}$$

Taking the Mellin moment (62) of both sides (with $s = \gamma$), we obtain

$$\gamma\, \tilde{g}(\omega,\gamma) \;=\; \frac{\tilde{P}_{gg}(\omega)}{2\pi}\, \widetilde{\alpha_s g}(\omega,\gamma)\,. \tag{B14}$$

Thus, after inserting relation (B7) we find

$$\widetilde{\alpha_s g}(\omega,\gamma) \;=\; \frac{2\pi\tilde{g}_0(\omega)}{\tilde{P}_{gg}(\omega)}\, \gamma^{-\frac{b_0}{2\pi}\bar{P}_{gg}(\omega)} \tag{B15}$$

which after coming back to the x variable reads

$$\widetilde{\alpha_s g}(x,\gamma) \;=\; \int \frac{d\omega}{2\pi i}\, x^{-\omega}\, \frac{2\pi\tilde{g}_0(\omega)}{\tilde{P}_{gg}(\omega)}\, \gamma^{-\frac{b_0}{2\pi}\bar{P}_{gg}(\omega)}\,. \tag{B16}$$

Both functions have logarithmic cut singularity in the complex γ-plane with the branch point at $\gamma = 0$.

---

[1] A. P. Bukhvostov, G. V. Frolov, L. N. Lipatov and E. A. Kuraev, Nucl. Phys. B **258** (1985) 601.
[2] R. K. Ellis, W. Furmanski and R. Petronzio, Nucl. Phys. B **207** (1982) 1.
[3] R. K. Ellis, W. Furmanski and R. Petronzio, Nucl. Phys. B **212** (1983) 29.
[4] J. Bartels, Phys. Lett. B **298** (1993) 204.
[5] J. Bartels, Z. Phys. C **60** (1993) 471.

[6] J. Bartels and M. G. Ryskin, Z. Phys. C **60** (1993) 751.
[7] J. Bartels and M. G. Ryskin, Z. Phys. C **62** (1994) 425.
[8] V. M. Braun, A. N. Manashov and J. Rohrwild, arXiv:0908.1684 [hep-ph].
[9] A. D. Martin, R. G. Roberts, W. J. Stirling and R. S. Thorne, Phys. Lett. B **443** (1998) 301.
[10] A. D. Martin and M. G. Ryskin, Phys. Lett. B **431** (1998) 395.
[11] J. Bartels, K. J. Golec-Biernat and K. Peters, Eur. Phys. J. C **17** (2000) 121.
[12] K. J. Golec-Biernat and M. Wüsthoff, Phys. Rev. D **59** (1999) 014017.
[13] K. J. Golec-Biernat and M. Wüsthoff, Phys. Rev. D **60** (1999) 114023.
[14] A. M. Staśto, K. J. Golec-Biernat and J. Kwieciński, Phys. Rev. Lett. **86** (2001) 596.
[15] J. Bartels, K. J. Golec-Biernat and H. Kowalski, Phys. Rev. D **66** (2002) 014001.
[16] A. Glazov [H1 collaboration], a contribution to the XVII International Workshop on Deep-Inelastic Scattering and Related Subjects, DIS 2009, 26-30 April 2009, Madrid; arXiv:0911.0159 [hep-ex].
[17] J. Bartels and M. Wüsthoff, Z. Phys. C **66** (1995) 157.
[18] J. Bartels and C. Bontus, Phys. Rev. D **61** (2000) 034009.
[19] L. N. Lipatov, Nucl. Phys. B **452** (1995) 369.
[20] M. Hentschinski, arXiv:0908.2576 [hep-ph].
[21] L. N. Lipatov, Sov. J. Nucl. Phys. **23** (1976) 338 [Yad. Fiz. **23** (1976) 642].
[22] E. A. Kuraev, L. N. Lipatov and V. S. Fadin, Sov. Phys. JETP **45** (1977) 199 [Zh. Eksp. Teor. Fiz. **72** (1977) 377].
[23] I. I. Balitsky and L. N. Lipatov, Sov. J. Nucl. Phys. **28** (1978) 822 [Yad. Fiz. **28** (1978) 1597].
[24] L. N. Lipatov, Phys. Rept. **286** (1997) 131.
[25] L. N. Lipatov, Sov. Phys. JETP **63** (1986) 904 [Zh. Eksp. Teor. Fiz. **90** (1986) 1536].
[26] I. Balitsky, Nucl. Phys. B **463** (1996) 99.
[27] Y. V. Kovchegov, Phys. Rev. D **60** (1999) 034008.
[28] Y. V. Kovchegov, Phys. Rev. D **61** (2000) 074018.
[29] J. Bartels and C. Ewerz, JHEP **9909** (1999) 026.
[30] J. Bartels and K. Kutak, Eur. Phys. J. C **53** (2008) 533.
[31] N. N. Nikolaev and B. G. Zakharov, Z. Phys. C **49** (1991) 607.
[32] C. D. White and R. S. Thorne, Phys. Rev. D **75** (2007) 034005.
[33] A. D. Martin, W. J. Stirling, R. S. Thorne and G. Watt, Eur. Phys. J. C **63** (2009) 189.
[34] H. Kowalski, L. Motyka and G. Watt, Phys. Rev. D **74** (2006) 074016.
[35] S. J. Brodsky, A. Hebecker and E. Quack, Phys. Rev. D **55** (1997) 2584; J. Raufeisen, J. C. Peng and G. C. Nayak, Phys. Rev. D **66** (2002) 034024; M. A. Betemps, M. B. G. Ducati, M. V. T. Machado and J. Raufeisen, Phys. Rev. D **67** (2003) 114008; B. Z. Kopeliovich, J. Raufeisen and A. V. Tarasov, Phys. Lett. B **503** (2001) 91; B. Z. Kopeliovich, A. H. Rezaeian, H. J. Pirner and I. Schmidt, Phys. Lett. B **653** (2007) 210.
[36] C. S. Lam and W. K. Tung, Phys. Rev. D **18** (1978) 2447; Phys. Lett. B **80** (1979) 228; Phys. Rev. D **21** (1980) 2712.
[37] R. J. Fries, B. Muller, A. Schafer and E. Stein, Phys. Rev. Lett. **83** (1999) 4261; R. J. Fries, A. Schafer, E. Stein and B. Muller, Nucl. Phys. B **582** (2000) 537; F. Gelis and J. Jalilian-Marian, Phys. Rev. D **66** (2002) 094014; F. Gelis and J. Jalilian-Marian, Phys. Rev. D **76** (2007) 074015.